DIGITAL ACCESS TO SCHOLARSHIP AT HARVARD
DASH.HARVARD.EDU

HARVARD LIBRARY

Mitophagy of damaged mitochondria occurs locally in distal neuronal axons and requires PINK1 and Parkin

Citation

Ashrafi, Ghazaleh, Julia S. Schlehe, Matthew J. LaVoie, and Thomas L. Schwarz. 2014. "Mitophagy of damaged mitochondria occurs locally in distal neuronal axons and requires PINK1 and Parkin." The Journal of Cell Biology 206 (5): 655-670. doi:10.1083/jcb.201401070. http://dx.doi.org/10.1083/jcb.201401070.

Published version

https://doi.org/10.1083/jcb.201401070

Link

http://nrs.harvard.edu/urn-3:HUL.InstRepos:14351293

Terms of use

This article was downloaded from Harvard University's DASH repository, and is made available under the terms and conditions applicable to Other Posted Material (LAA), as set forth at
https://harvardwiki.atlassian.net/wiki/external/NGY5NDE4ZjgzNTc5NDQzMGIzZWZhMGFlOWI2M2EwYTg

Accessibility

https://accessibility.huit.harvard.edu/digital-accessibility-policy

Share Your Story

The Harvard community has made this article openly available.
Please share how this access benefits you. Submit a story

THE JOURNAL OF CELL BIOLOGY

Mitophagy of damaged mitochondria occurs locally in distal neuronal axons and requires PINK1 and Parkin

Ghazaleh Ashrafi,[1,2] Julia S. Schlehe,[3] Matthew J. LaVoie,[3] and Thomas L. Schwarz[2]

[1]Department of Molecular and Cellular Biology, Harvard University, Cambridge, MA 02138
[2]F.M. Kirby Neurobiology Center, Children's Hospital Boston, Boston, MA 02115
[3]Center for Neurological Diseases, Brigham and Women's Hospital, Boston, MA 02115

To minimize oxidative damage to the cell, malfunctioning mitochondria need to be removed by mitophagy. In neuronal axons, mitochondrial damage may occur in distal regions, far from the soma where most lysosomal degradation is thought to occur. In this paper, we report that PINK1 and Parkin, two Parkinson's disease–associated proteins, mediate local mitophagy of dysfunctional mitochondria in neuronal axons. To reduce cytotoxicity and mimic physiological levels of mitochondrial damage, we selectively damaged a subset of mitochondria in hippocampal axons. Parkin was rapidly recruited to damaged mitochondria in axons followed by formation of LC3-positive autophagosomes and LAMP1-positive lysosomes. In *PINK1*$^{-/-}$ axons, damaged mitochondria did not accumulate Parkin and failed to be engulfed in autophagosomes. Similarly, initiation of mitophagy was blocked in *Parkin*$^{-/-}$ axons. Our findings demonstrate that the PINK1–Parkin-mediated pathway is required for local mitophagy in distal axons in response to focal damage. Local mitophagy likely provides rapid neuroprotection against oxidative stress without a requirement for retrograde transport to the soma.

Introduction

Parkinson's disease (PD) is the second most common neurodegenerative disease and is closely associated with mitochondrial dysfunction (Chen and Chan, 2009). Mitochondria, particularly when dysfunctional, produce excessive reactive oxygen species (ROS; Wallace, 2005) and must be removed by quality control pathways. Two hereditary forms of early onset PD arise from mutations in PINK1 (PTEN-induced putative kinase 1), a Ser/Thr kinase, and Parkin, an E3 ubiquitin ligase. PINK1 and Parkin act sequentially in a pathway for selective autophagy of damaged mitochondria, also known as mitophagy (Narendra et al., 2008, 2010).

PINK1 functions as a sensor for mitochondrial damage; its precursor is constitutively imported to the inner membrane of healthy mitochondria, where it is proteolytically cleaved (Greene et al., 2012) and eventually degraded by the proteasome (Yamano and Youle, 2013). Loss of mitochondrial membrane potential prevents the import of PINK1 and leads to its accumulation on the mitochondrial outer membrane, where PINK1 recruits Parkin from the cytosol. Parkin, in turn, activates the autophagic machinery to engulf damaged mitochondria. In addition to its involvement in mitophagy, Parkin plays a PINK1-independent, antiapoptotic role by limiting the translocation of proapoptotic Bax to the mitochondrial surface (Johnson et al., 2012a) and increasing the threshold for cytochrome *c* release from mitochondria (Berger et al., 2009), both under normal and stress conditions (Johnson et al., 2012b).

The PINK1–Parkin pathway of mitophagy has been characterized mainly in immortalized and nonneuronal cell lines, whereas studies in primary neurons have produced contradictory results (Seibler et al., 2011; Van Laar et al., 2011; Cai et al., 2012; Rakovic et al., 2013). Specifically, it remains controversial in neurons whether Parkin is recruited to depolarized mitochondria and whether endogenous Parkin is sufficient to trigger mitophagy. This ambiguity may arise from the use of potent chemical uncouplers, such as carbonyl cyanide 3-chlorophenylhydrazone

Correspondence to Thomas L. Schwarz: Thomas.schwarz@childrens.harvard.edu

Abbreviations used in this paper: CCCP, carbonyl cyanide 3-chlorophenylhydrazone; CMV, cytomegalovirus; DIV, day in vitro; mt-KR, mitochondrial KillerRed; PD, Parkinson's disease; ROS, reactive oxygen species; TMRM, tetramethylrhodamine, methyl ester.

© 2014 Ashrafi et al. This article is distributed under the terms of an Attribution–Noncommercial–Share Alike–No Mirror Sites license for the first six months after the publication date (see http://www.rupress.org/terms). After six months it is available under a Creative Commons License (Attribution–Noncommercial–Share Alike 3.0 Unported license, as described at http://creativecommons.org/licenses/by-nc-sa/3.0/).

The Rockefeller University Press $30.00
J. Cell Biol. Vol. 206 No. 5 655–670
www.jcb.org/cgi/doi/10.1083/jcb.201401070

(CCCP), to induce nonphysiological levels of mitochondrial damage (Grenier et al., 2013). Unlike many cell lines where the entire mitochondrial network can be cleared by mitophagy (Narendra et al., 2008, 2010; Geisler et al., 2010), neurons are strictly dependent on mitochondrial ATP production (Almeida et al., 2001, 2004). Neuronal studies of mitophagy may therefore require more physiological methods for induction of mitochondrial damage.

Neurons face unique challenges with respect to mitochondrial quality control. Most neuronal mitochondria reside in distal dendritic and axonal processes, far from the cell body where lysosomes are abundant (Parton et al., 1992; Craig and Banker, 1994). Despite several lines of evidence supporting the presence of mature and functional lysosomes in axons (Lee et al., 2011, Maday et al., 2012), it is still debated whether efficient degradation of organelles can occur in distal processes (Cai et al., 2012). Indeed, most studies have focused on mitochondrial quality control in the soma (Seibler et al., 2011; Van Laar et al., 2011; Cai et al., 2012; Rakovic et al., 2013), and little is known about mitochondrial clearance from distal axons. Quality control of axonal mitochondria, however, is of particular interest because axonal degeneration precedes the loss of the soma in neurodegenerative diseases, such as PD (Burke and O'Malley, 2013). Two studies have reported that depolarized mitochondria may be preferentially transported in retrograde direction toward the soma to be degraded (Miller and Sheetz, 2004; Cai et al., 2012). Others, however, did not find a correlation between mitochondrial membrane potential and the direction of motility (Verburg and Hollenbeck, 2008). Furthermore, it is not immediately clear that the PINK1–Parkin model of nonneuronal mitophagy would be applicable to distal axons because substantial rates of axonal transport or local synthesis of PINK1 would be necessary to sustain rapid turnover of PINK1 on healthy mitochondria.

We recently found that mitochondrial damage arrested motility through degradation of the mitochondrial motor adaptor protein Miro in a pathway mediated by PINK1 and Parkin (Wang et al., 2011). This observation suggested that dysfunctional mitochondria would not move back to the soma and instead might undergo local mitophagy in distal axons to prevent further spread of oxidative damage. Here, we damage a small subset of axonal mitochondria in hippocampal axons to mimic physiological levels of mitochondrial dysfunction. We observe rapid and local recruitment of Parkin, LC3-positive autophagosomes, and LAMP1 (lysosomal-associated membrane protein 1)-positive lysosomes to damaged mitochondria. We show that endogenous PINK1 and Parkin are both required for axonal mitophagy, indicating that this pathway functions locally in distal neuronal axons.

Results

Activation of mitochondrial KillerRed (mt-KR) affects mitochondrial morphology in axons

To study mitophagy in neurons, we set out to induce mitochondrial damage in a spatiotemporally controlled manner, while preserving the overall integrity of the mitochondrial network.

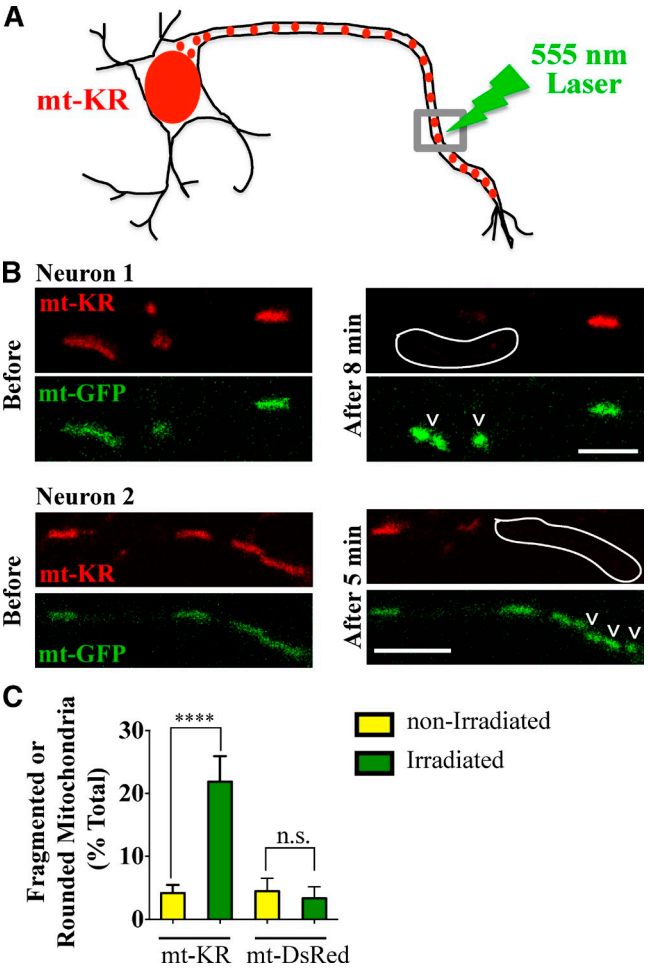

Figure 1. **Activation of mt-KR in neuronal axons.** (A) mt-KR was expressed in hippocampal neurons and activated locally with a 555-nm laser. (B) Two axons expressing mt-KR and mt-GFP before and after irradiation and concomitant photobleaching of mt-KR in the outlined regions. Mitochondria became rounded and fragmented (arrowheads), and their GFP fluorescence intensity increased. Image acquisition settings were kept constant before and after KillerRed activation. (C) Morphological changes in mitochondria expressing mt-KR or mt-DsRed were quantified. n = 88–109 irradiated and n = 293–448 nonirradiated mitochondria from 12–15 transfections. ****, $P < 0.0001$. Error bars represent means ± SEM. Bars, 5 µm.

To this end, mt-KR, a genetically encoded photosensitizer targeted to mitochondria, was used to selectively damage a subset of axonal mitochondria. Light-induced activation of mt-KR causes local ROS-mediated damage to mitochondria (Bulina et al., 2006; Ertürk et al., 2014) and has been previously used to induce mitophagy in HeLa cells (Yang and Yang, 2011; Wang et al., 2012). We expressed mt-KR in rat hippocampal neurons and, with a 555-nm laser, irradiated a 10-µm section of an axon, which typically included three to four mitochondria, to activate and thereby photobleach mt-KR in those mitochondria, while sparing those in adjacent segments (Fig. 1 A). Mitochondrial damage results in stereotypical changes in mitochondrial morphology, such as swelling and fragmentation (Legros et al., 2002; Kaasik et al., 2007). To observe mitochondrial morphology after mt-KR photobleaching, we coexpressed mitochondrially targeted GFP (mt-GFP). Within 10 min of mt-KR activation, a fragmented or rounded morphology arose

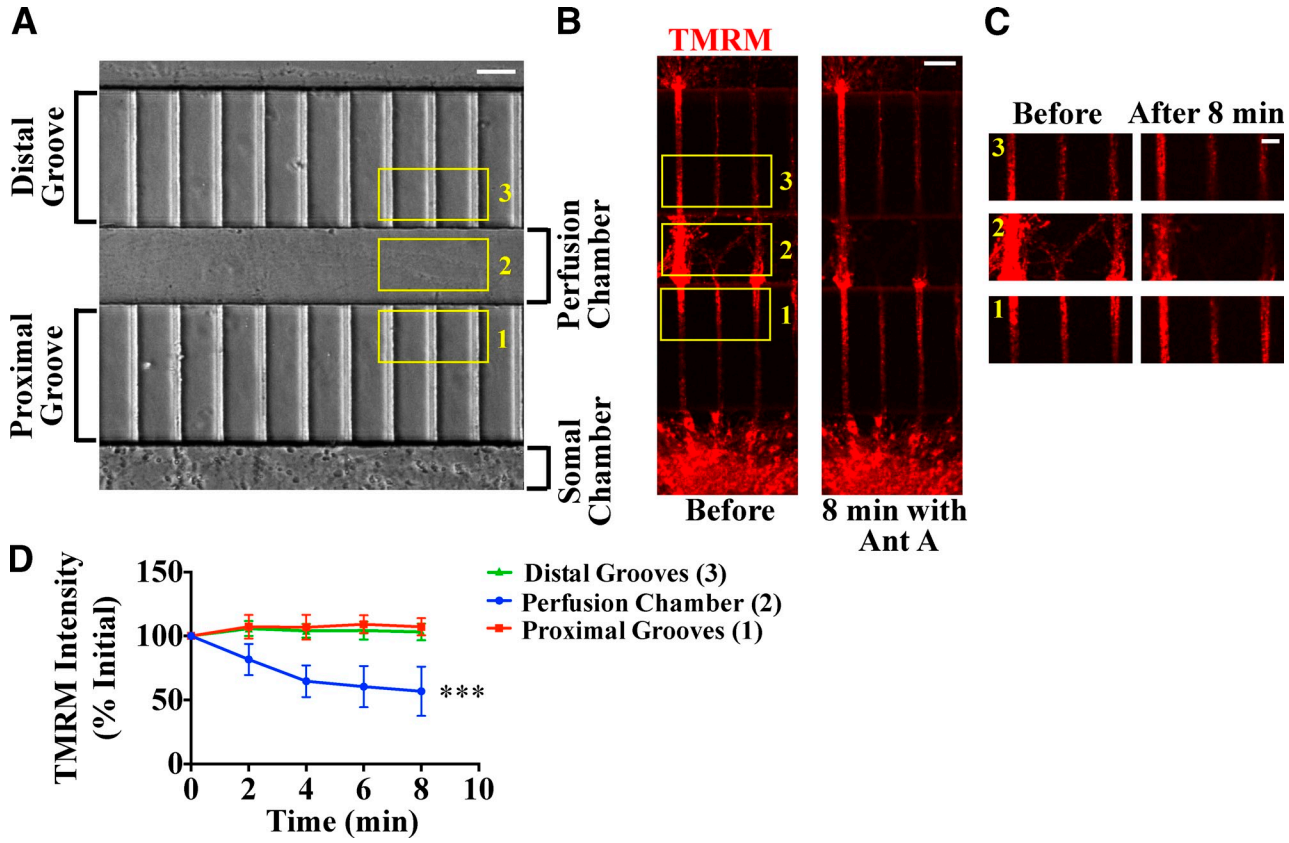

Figure 2. **Localized depolarization of axonal mitochondria in microfluidic devices.** (A–C) Neurons were plated in the somal chamber (A), and axons grew through two sets of 200-µm microgrooves intersected by a 100-µm-long perfusion channel (B) and enlarged areas in C. Addition of 40 µM Antimycin A (Ant A) to the perfusion channel (box 2) decreased mitochondrial TMRM staining in that chamber, whereas mitochondria in the proximal and distal microgrooves (boxes 1 and 3) remained polarized. (D) Relative TMRM intensity, normalized to $t = 0$, as a function of time after addition of Antimycin A. The change in TMRM intensity is statistically significant only in the perfusion chamber. ***, $P < 0.001$ by linear regression analysis; $n = 4$ microfluidic devices. Error bars represent means ± SEM. Bars: (A and B) 50 µm; (C) 20 µm.

in 22% of the laser-illuminated mitochondria compared with 4% of the mitochondria outside the illuminated region ($P < 0.0001$; Fig. 1, B and C). In contrast, irradiation of mitochondria expressing mitochondrially targeted DsRed (mt-DsRed) did not cause fragmentation or rounding (Fig. S1 A). Activation of mt-KR also increased the fluorescence intensity of mt-GFP within those mitochondria (Fig. 1 B), possibly because of dequenching of the fluorophores in the swollen matrix of damaged mitochondria. Consistent with oxidative damage as the mechanism of mt-KR, we rarely detected changes in mitochondrial morphology when mt-KR was activated in Hibernate E medium, which contains antioxidants.

Localized depolarization of axonal mitochondria in microfluidic devices

Although mt-KR can restrict damage to a few mitochondria, quantitative examination of mitophagy required damage to a larger population of axonal mitochondria, while still sparing the majority of mitochondria in a neuron. To this end, we took advantage of microfluidic local perfusion chambers (Taylor et al., 2010). Fluidic isolation of compartments in these devices allows for the selective pharmacological manipulation of a subset of axonal mitochondria. Hippocampal neurons were plated in the somal compartment and extended axons through two sets of 200-µm-long microgrooves that were separated by a 100-µm-long perfusion chamber (Fig. 2 A).

The ionophore CCCP is frequently used in cell lines to activate mitophagy; however, it is highly toxic to neurons. We therefore used Antimycin A, an inhibitor of respiratory complex III (Slater, 1973), to impair mitochondria. Antimycin A induces mitochondrial ROS production in nonneuronal cells (Soubannier et al., 2012a) and depolarizes neuronal mitochondria (Cai et al., 2012). Applying 40 µM Antimycin A to the perfusion chamber decreased tetramethylrhodamine, methyl ester (TMRM) intensity, a measure of mitochondrial membrane potential, to 57% of its initial value within 8 min (Fig. 2, B–D). Loss of TMRM intensity was less prominent in thickly bundled axons, presumably as a result of limited access of the drug (Fig. 2, B and C). TMRM fluorescence did not change in axons within the grooves leading to or from the perfusion chamber. Thus, mitochondrial depolarization could be restricted to the perfusion chamber.

Mito-KR activation and Antimycin A cause axonal mitochondria to colocalize with autophagosomes

It has been reported that damaged mitochondria move retrograde toward the soma, presumably, to undergo mitophagy there (Miller and Sheetz, 2004; Cai et al., 2012). However,

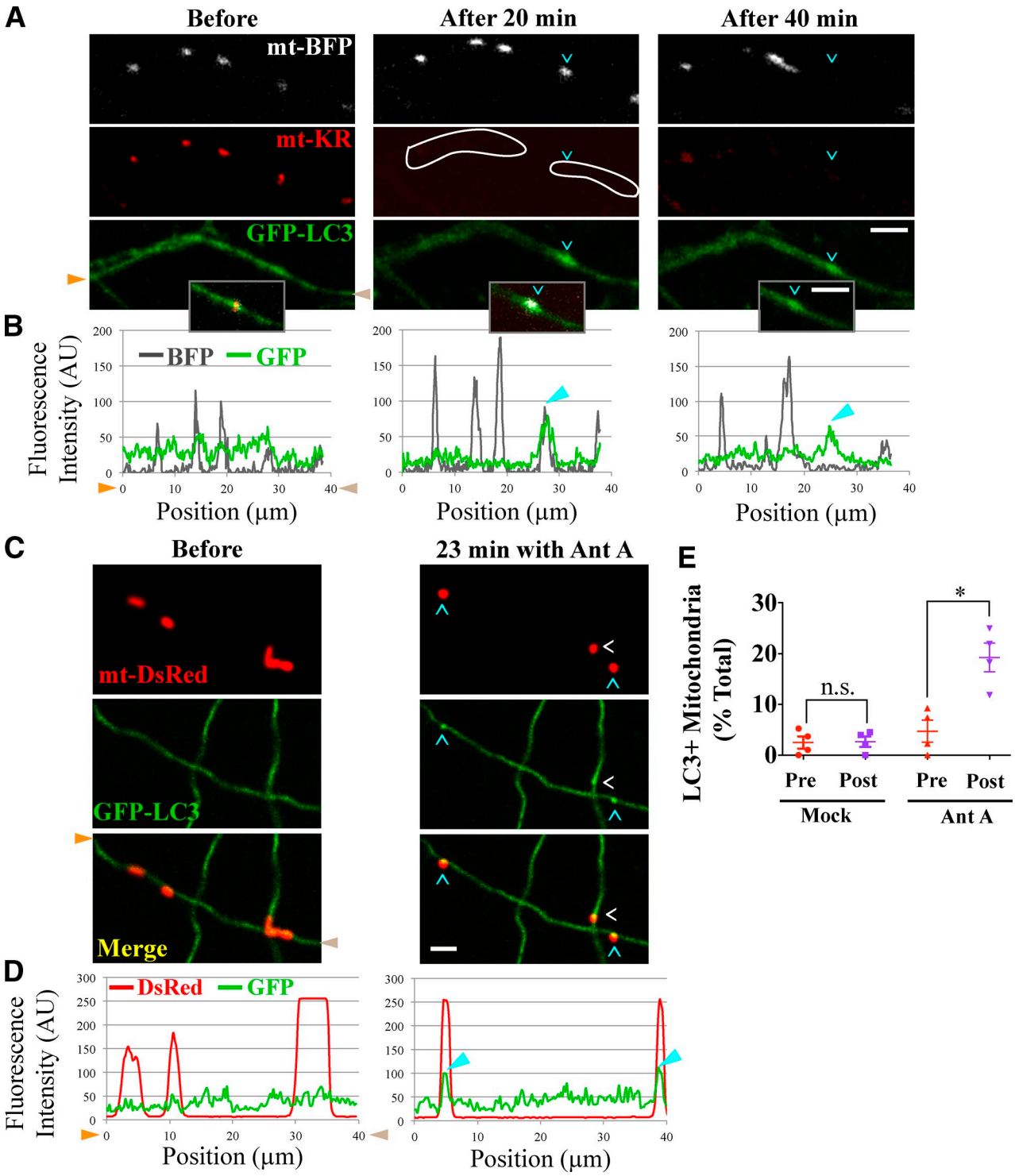

Figure 3. **Damaged axonal mitochondria colocalize with autophagosomes.** (A–D) Cyan and white arrowheads denote GFP-LC3–positive autophagosomes colocalizing with mitochondria. (A) Within the outlined laser-illuminated region of activated mt-KR, one mt-BFP–labeled mitochondrion colocalized with a GFP-LC3–positive autophagosome; the BFP signal from the engulfed mitochondrion was present 20 min after illumination but disappeared by 40 min, even though the autophagosome was present. In the insets are the merged images for the engulfed mitochondrion. (B) Line scan analysis of A. (C) GFP-LC3–positive autophagosomes formed on mitochondria depolarized with 40 μM Antimycin A (Ant A) in the perfusion chamber of a microfluidic device. (D) Line scan analysis of C. Here and subsequently, orange and brown arrowheads denote corresponding points in images and line scans, and mitochondria marked with cyan arrowheads correspond to similarly marked peaks in line scans. (E) Frequency of autophagosome formation before and after Antimycin A or mock treatments. n = 182–244 mitochondria from four microfluidic devices per condition. Here and in subsequent graphs, each point represents the average percentage of positive mitochondria for a single microfluidic chamber. *, $P < 0.05$. Error bars represent means ± SEM. AU, arbitrary unit. Bars, 5 μm.

our observations of mitochondrial motility arrest (Wang et al., 2011) and the accumulation of aged mitochondrial proteins in distal processes (Ferree et al., 2013) argue against this model. In addition, a recent study has shown autophagosome formation in distal regions of undamaged neurons in culture (Maday et al., 2012). To determine whether damaged mitochondria in distal axons could locally recruit autophagosomes, we expressed the autophagosome marker GFP-LC3 along with mt-KR in hippocampal neurons. GFP-LC3 is a cytosolic protein, but upon induction of autophagy, it gets lipidated and incorporated into autophagosomes forming distinct puncta (Mizushima and Komatsu, 2011). Mitochondrially targeted BFP (mt-BFP) was also expressed to mark mitochondria. After activation of mt-KR, we observed GFP-LC3 accumulation on mitochondria, indicating the formation of mitochondrion-containing autophagosomes (Fig. 3, A and B). In some instances, the autophagosomal mitochondrion eventually disappeared, presumably, as a result of the formation of autolysosomes. Our findings establish that the initial stages of mitophagy, specifically colocalization with LC3-positive autophagosomes, can occur locally in axons.

To further examine initiation of mitophagy, we turned to microfluidic devices and sparsely transfected neurons with GFP-LC3 and mt-DsRed so that individually labeled axons could be visualized before and after depolarization of mitochondria with Antimycin A (Fig. 3, C and D). 40 µM Antimycin A increased the fraction of mitochondria colocalized with distinct GFP-LC3 puncta from 5 to 20% ($P < 0.05$; Fig. 3 E). This percentage represents the maximum fraction of GFP-LC3–positive mitochondria observed at any single point during imaging. Because of the asynchronous rate of autophagosome formation and degradation, the integrated sum of all the mitochondria engulfed by autophagosomes is likely to be higher. In mock experiments in which the solution in the perfusion chamber did not contain Antimycin A, there was no increase in the percentage of mitochondria positive for GFP-LC3 ($P = 1$; Fig. 3 E). The accumulation of GFP-LC3 at mitochondrial sites was not an artifact as a result of possible local axon swelling because cytoplasmic EGFP did not accumulate in the vicinity of mitochondria after either mt-KR activation or Antimycin A treatment (Fig. S1, B–E). Axonal morphology was also unaffected by the accumulation of RFP-LC3 on depolarized mitochondria (Fig. S1, D and E). We therefore conclude that mitophagy of damaged mitochondria is initiated in distal axons.

Axonal lysosomes colocalize with autophagosomes containing damaged mitochondria

Degradation of autophagosomal cargoes requires fusion of autophagosomes with lysosomes to form autolysosomes (Xie and Klionsky, 2007), and it was suggested that autophagosomes would have to translocate to neuronal soma to fuse with lysosomes (Cai et al., 2012). Imaging of GFP-LC3 puncta in distal axons treated with Antimycin A (Fig. 3, C–E) indicated that 76% of nonmitochondrial autophagosomes were mobile, whereas only 13% of mitoautophagosomes moved; local autolysosome formation therefore appeared likely. To examine endogenous lysosome distribution, dissociated hippocampal neurons were immunostained for LAMP1, a late endosome/lysosome marker. We observed numerous LAMP1-positive vesicles in axons (Fig. S2 A). Expression of YFP-tagged LAMP1 indicated that 40% of axonal lysosomes were motile and moved bidirectionally (Fig. S2, B and C) as previously observed (Maday et al., 2012).

To determine whether these lysosomes would be recruited to autophagosomes containing mitochondria, hippocampal neurons were plated in microfluidic devices and sparsely transfected with mt-BFP, RFP-LC3, and LAMP1-YFP. RFP-LC3 is more stable than GFP-LC3 and labels both autophagosomes and autolysosomes (Bains and Heidenreich, 2009), accounting for frequent double labeling of lysosomes with both LAMP1-YFP and RFP-LC3. 50 min after application of Antimycin A to the perfusion chamber, the fraction of axonal mitochondria colocalizing with RFP-LC3–positive vesicles increased from 5% before treatment to 20% after ($P < 0.05$; Fig. 4, A–C). Similarly, mitochondrial colocalization increased significantly with vesicles containing either LAMP1-YFP alone (from 9 to 28%, $P < 0.01$) or containing both RFP-LC3 and LAMP1-YFP (from 5 to 19%, $P < 0.05$). In neurons preincubated with lysosomal inhibitors (5 µM pepstatin A and 10 µM E64D) to prevent the loss of mitochondrial markers after autophagolysosome formation, 60% of mitochondria became LAMP1-YFP–positive after Antimycin A treatment ($P < 0.05$; Fig. 4 C). Thus, local lysosomal degradation of mitochondria was rapid and extensive. In one example of live imaging (Fig. 4, D and E), an RFP-LC3–positive autophagosome first formed on a fragmented mitochondrion 25 min after the addition of Antimycin A. Then, a moving RFP-LC3– and LAMP1-YFP–positive lysosome stopped at the site of the autophagosome-associated mitochondrion. 17 min later, the mitochondrial BFP signal was significantly diminished, which could indicate acidification of the autolysosome or degradation of its mitochondrial content, but was not cause by photobleaching of mt-BFP because other mitochondria in the field retained their BFP fluorescence (Fig. 4, F and G). Thus, mobile axonal lysosomes are recruited to autophagosomes to mediate local degradation of their damaged mitochondrial content.

Axonal mitophagy requires Parkin recruitment to axonal mitochondria

In nonneuronal cells, mitochondrial depolarization causes recruitment of Parkin from the cytoplasm to the mitochondrial outer membrane where it promotes the onset of mitophagy (Narendra et al., 2008; Geisler et al., 2010). In neurons, Parkin translocation has been reported in the cell bodies of neurons treated with CCCP or valinomycin (Seibler et al., 2011; Cai et al., 2012) but was not observed in axons treated with CCCP (Van Laar et al., 2011; Cai et al., 2012). We, in contrast, had observed accumulation of Parkin on axonal mitochondria in response to global depolarization with Antimycin A (Wang et al., 2011). Because axonal Parkin recruitment might be obscured by either overexpression of YFP-Parkin in the cytosol, excessively toxic exposure to CCCP, or failure to observe the recruitment before rapid mitophagy, we reexamined the question with locally restricted and near-physiological levels of

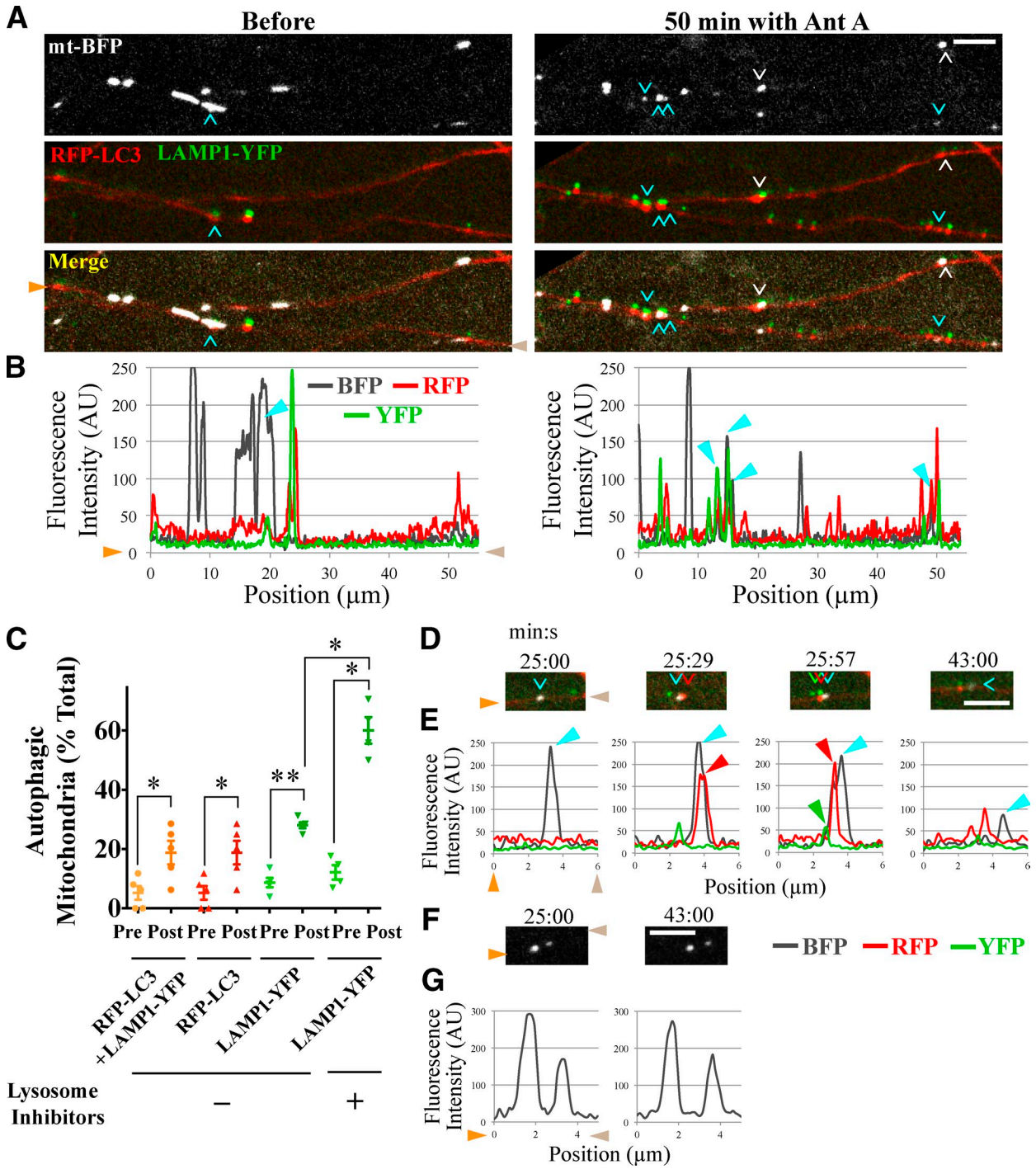

Figure 4. **Axonal lysosomes are recruited to autophagosomes containing damaged mitochondria.** (A) RFP-LC3 and LAMP1-YFP–positive autolysosomes colocalize with mitochondria depolarized with 40 μM Antimycin A (Ant A). Arrowheads (cyan in the top axon and white in the bottom axon) denote LC3- and LAMP1-positive mitochondria. (B) Line scan analysis of the upper axon in A. Peaks marked by arrowheads correspond to those with cyan arrowheads in A. (C) Frequency of mitochondrial colocalization with autophagosome and lysosome markers before and 50 min after Antimycin A addition to neurons with or without preincubation with lysosomal inhibitors Pepstatin A and E64d. n = 98–171 mitochondria from five microfluidic devices. *, $P < 0.05$; **, $P < 0.001$. (D and E) Time-lapse images starting 25 min after application of Antimycin A depict an RFP-LC3–positive autophagosome (red arrowheads) forming on a fragmented mitochondrion (cyan arrowheads). A moving LAMP1-YFP–positive lysosome (green arrowhead) stopped at the mitochondrion, and the mitochondrial signal subsequently diminished. (F and G) Neighboring mitochondria imaged in the same field as D retained their BFP signal. Orange and brown arrowheads denote corresponding points in images and line scans. Error bars represent means ± SEM. AU, arbitrary unit. Bars, 5 μm.

mitochondrial damage 20 min after irradiation of mitochondria expressing mt-KR and mt-BFP with 555 nm of light. When expressed at high levels, YFP-Parkin localizes to mitochondria and arrests their motility even in the absence of mitochondrial damage (Wang et al., 2011). At low levels, however, YFP-Parkin was diffuse in the axonal cytoplasm with only minor enrichment on a few mitochondria (Fig. 5, A and B). After activation of mt-KR, YFP-Parkin accumulated on 10% of the

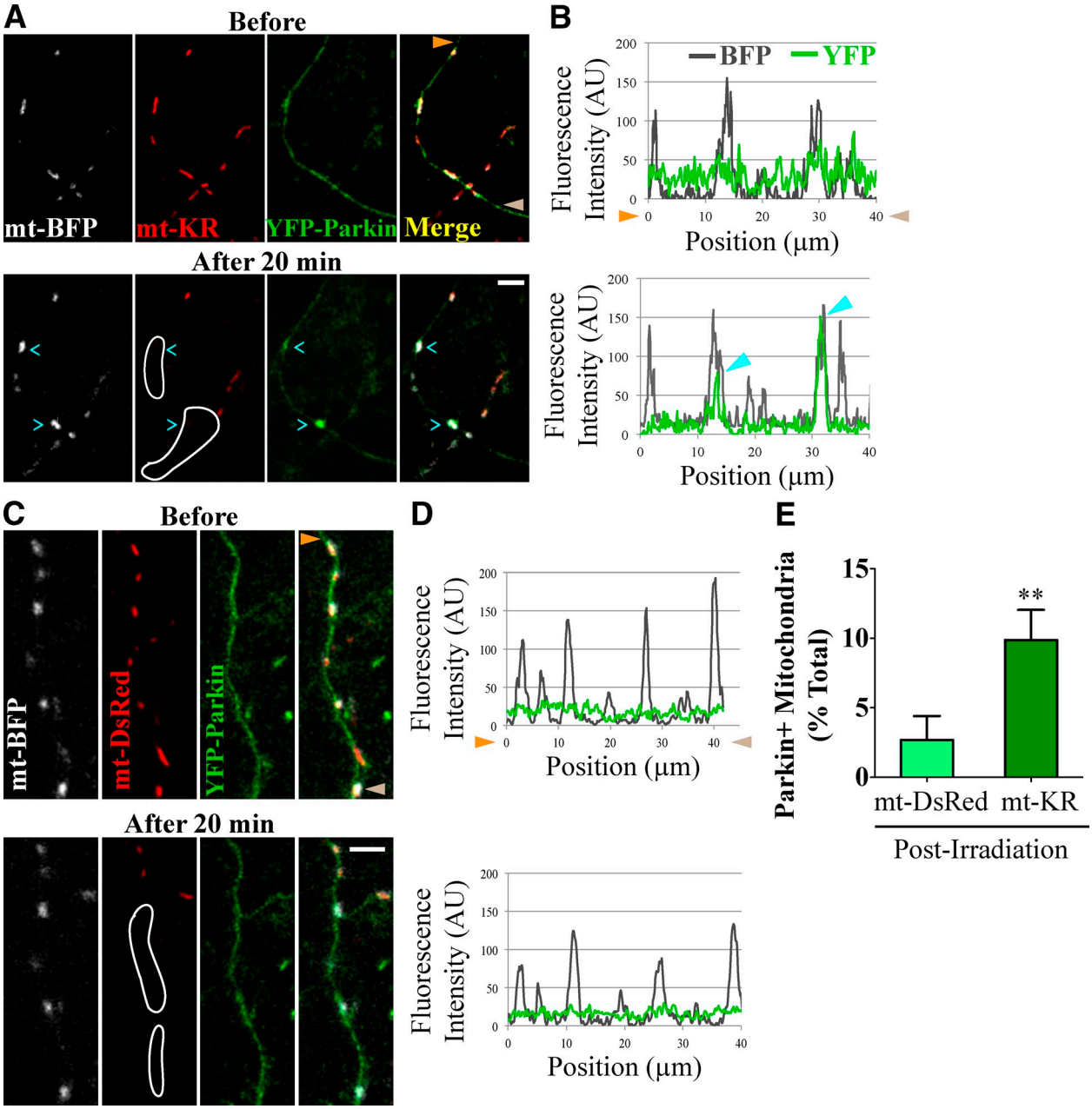

Figure 5. **Parkin is recruited to axonal mitochondria damaged with mt-KR.** (A) YFP-Parkin accumulates on a fraction of axonal mitochondria in the outlined area of mt-KR activation. (B) Line scan of the axon in A with cyan arrowheads marking two YFP-Parkin–positive mitochondria. (C and D) YFP-Parkin remained diffuse despite irradiation in the outlined area when mt-DsRed replaced mt-KR. Mitochondria with YFP-Parkin levels more than twice the background were scored as Parkin-positive here and in subsequent figures. Orange and brown arrowheads denote corresponding points in images and line scans. (E) Frequency of YFP-Parkin recruitment to irradiated mitochondria. n = 131–140 mitochondria from 12 transfections. **, $P < 0.001$. Error bars represent means ± SEM. AU, arbitrary unit. Bars, 5 μm.

targeted mitochondria that were previously Parkin negative (Fig. 5, A, B, and E). This recruitment was caused by ROS production by mt-KR; only 3% of mitochondria were Parkin positive after equivalent irradiation of mt-DsRed ($P < 0.01$; Fig. 5, C–E). Thus, local damage to a small subset of axonal mitochondria is sufficient to recruit Parkin selectively to the affected population.

To further examine the accumulation of Parkin on distal axonal mitochondria, we also used microfluidic devices with neurons transfected with mt-DsRed and YFP-Parkin. Depolarization of mitochondria with 40 μM Antimycin A led to substantial recruitment of YFP-Parkin to axonal mitochondria (Fig. 6, A and B); within 20 min, the percentage of Parkin-positive mitochondria increased from 5 to 40% ($P < 0.05$; Fig. 6 E). In mock experiments in which the perfusion chamber did not contain Antimycin A, there was no increase in YFP-Parkin–positive mitochondria ($P = 0.2$; Fig. 6 E).

Neither mt-KR nor Antimycin A recruited Parkin to all the targeted mitochondria. Indeed, activation of mt-KR resulted in loss of membrane potential in 45% of mitochondria, but

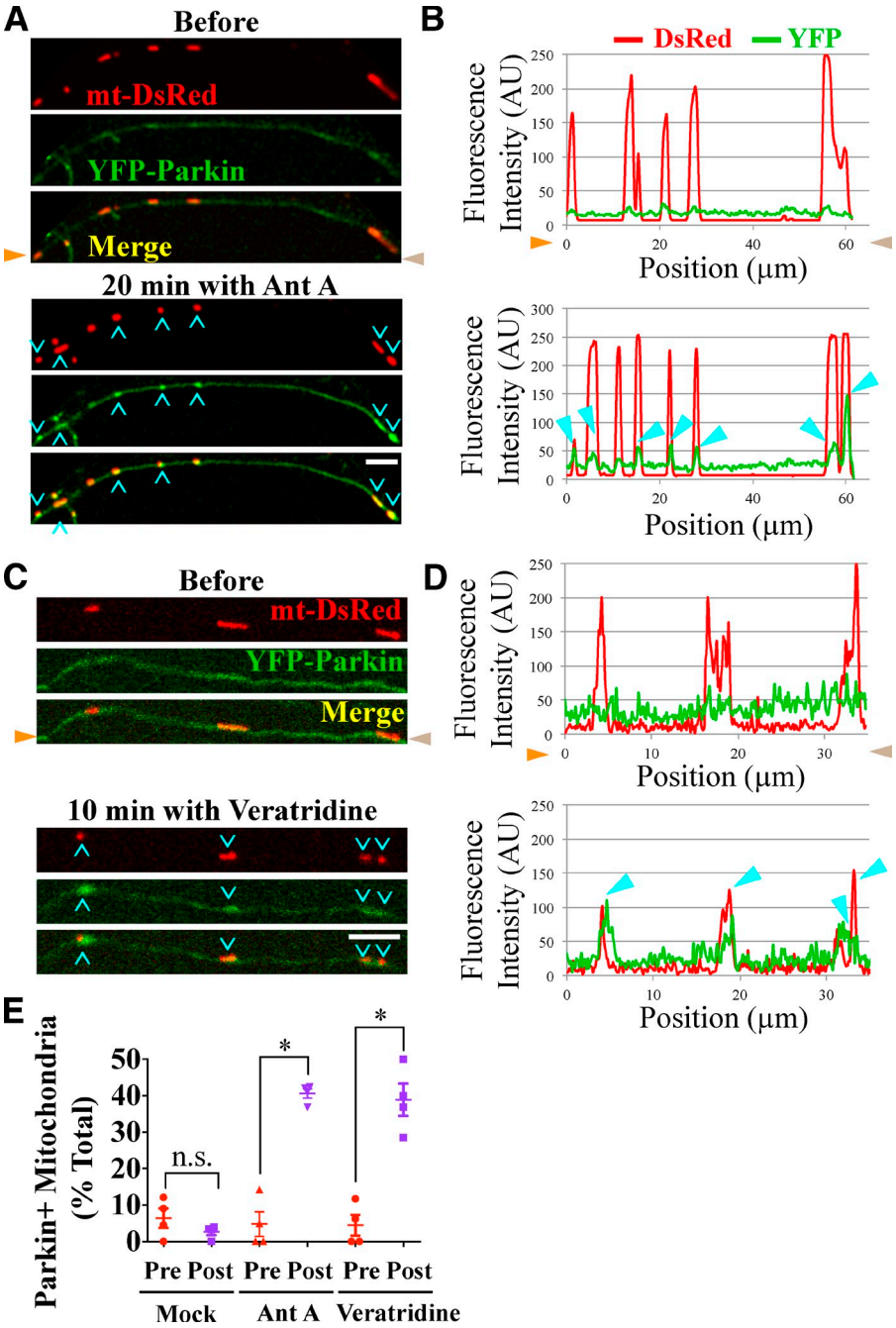

Figure 6. **Parkin recruitment by Antimycin A and Veratridine.** (A–D) Exposing axonal segments to 40 μM Antimycin A (Ant A; A and B) or 250 nM Veratridine (C and D) led to recruitment of YFP-Parkin to mitochondria (cyan arrowheads). Orange and brown arrowheads denote corresponding points in images and line scans. (E) Frequency of YFP-Parkin recruitment. n = 59–98 mitochondria from four microfluidic devices per condition. *, $P < 0.05$. Error bars represent means ± SEM. AU, arbitrary unit. Bars, 5 μm.

only 16% of those acquired YFP-Parkin (Fig. S3 A). Similarly, some but not all of the Antimycin A–depolarized mitochondria became Parkin positive (Fig. S3, B and C). Thus, loss of membrane potential is not sufficient to guaranty initiation of mitophagy, and other factors, including Parkin availability, may be limiting.

In several neurological diseases, such as PD, excessive neuronal firing is closely associated with neurodegeneration, and excitotoxicity-related increases in intracellular calcium can lead to ROS production and mitochondrial damage (Ambrosi et al., 2014). Therefore, we asked whether excitotoxic damage can trigger axonal mitophagy. Veratridine, an activator of voltage-gated sodium channels, was applied to axons to increase firing and intracellular calcium (Chang et al., 2006). Indeed, YFP-Parkin rapidly accumulated on 39% of mitochondria in the Veratridine-exposed region ($P < 0.05$; Fig. 6, C–E). Therefore, a stimulus that mimics a pathological insult also triggers activation of the Parkin pathway.

The recruitment of expressed Parkin to axonal mitochondria raised the question of whether endogenous Parkin was required for damage-induced mitophagy. We therefore compared mitophagy in hippocampal axons of *Parkin*$^{+/+}$ and *Parkin*$^{-/-}$ mice (Goldberg et al., 2003). In microfluidic chambers, GFP-LC3 was coexpressed with mt-DsRed to monitor autophagosome formation. In *Parkin*$^{+/+}$ axons, the fraction of mitochondria colocalizing with GFP-LC3–positive autophagosomes increased from 4% before to 33% after 35 min of Antimycin A treatment in the perfusion chamber ($P < 0.05$; Fig. 7,

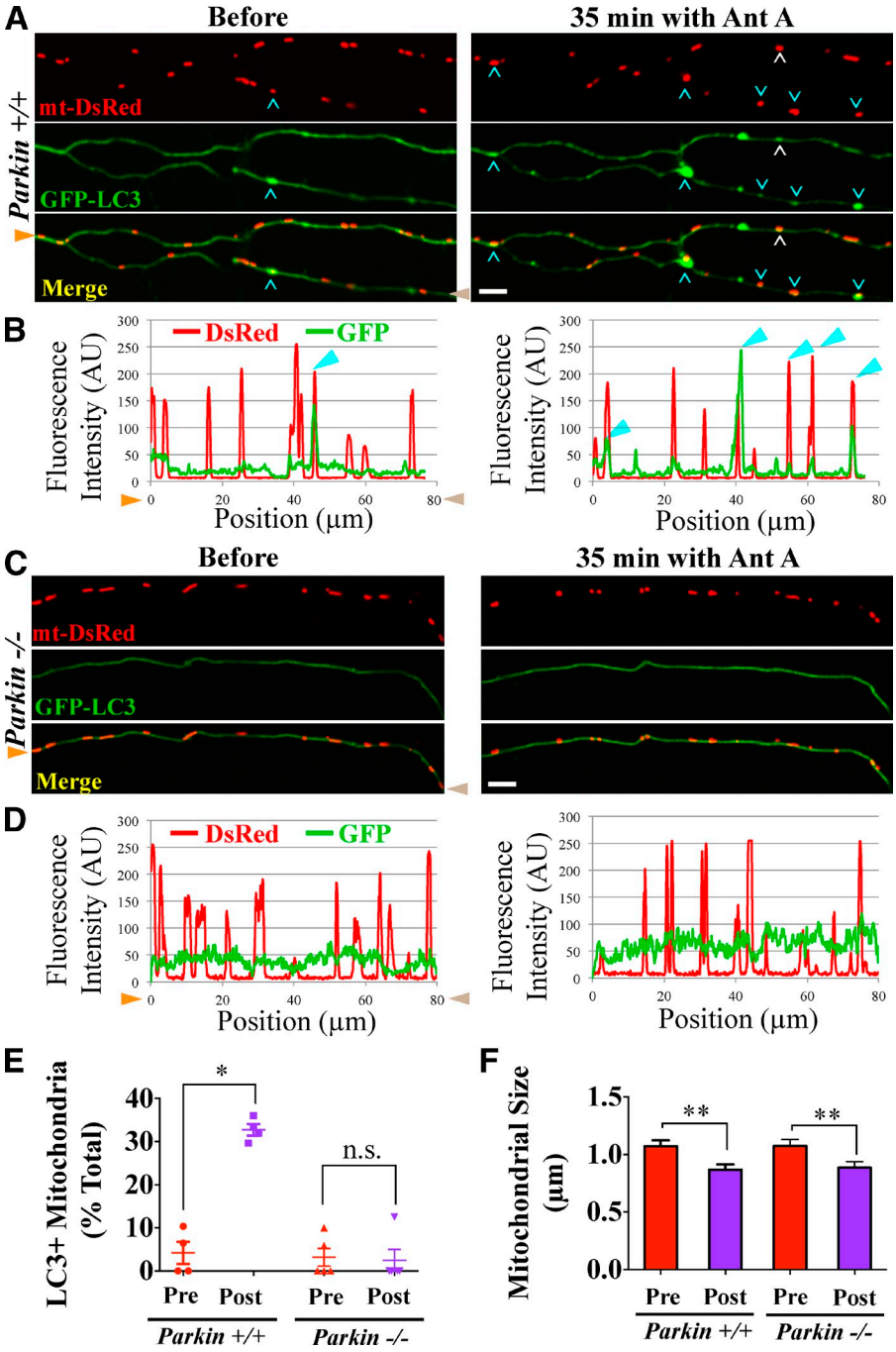

Figure 7. **Initiation of axonal mitophagy requires Parkin.** (A and B) GFP-LC3–positive autophagosomes (white and cyan arrowheads) form on mitochondria of *wild-type* (*Parkin*$^{+/+}$) axon segments treated with 20 μM Antimycin A (Ant A). Cyan arrowheads point to mitochondria in the axon analyzed in B. (C and D) In *Parkin*$^{-/-}$ axons, mitochondria did not acquire autophagosomes. Orange and brown arrowheads denote corresponding points in images and line scans. (E) Frequency of autophagosome formation axons before and after Antimycin A. n = 104–106 mitochondria from four to five microfluidic devices per genotype. (F) Quantification of mitochondrial size before and after 20 min of 20 μM Antimycin A treatment indicates that damage-induced mitochondrial remodeling is Parkin independent. The sizes of the fragmented mitochondria may be overestimates because of the limited resolution of the microscope. n = 76–99 mitochondria from four to five microfluidic devices per genotype. *, $P < 0.05$; **, $P < 0.001$. Error bars represent means ± SEM. AU, arbitrary unit. Bars, 5 μm.

A, B, and E). In contrast, in *Parkin*$^{-/-}$ axons, Antimycin A did not increase mitochondrial colocalization with autophagosomes ($P = 1$; Fig. 7, C–E). Damage-induced mitophagy could be rescued in *Parkin*$^{-/-}$ axons by expressing mCherry-Parkin (Fig. S4 A). Thus, depolarization-induced initiation of mitophagy in neuronal axons both triggers Parkin recruitment and requires Parkin. We also examined damage-induced mitochondrial fragmentation and found that treatment with Antimycin A for 20 min caused a significant decrease in mitochondrial size in both *Parkin*$^{+/+}$ and *Parkin*$^{-/-}$ axons ($P < 0.01$; Fig. 7 F). We conclude that Parkin is not required for the remodeling of depolarized mitochondria, only for the subsequent recruitment of the autophagosome.

Parkin and LC3 recruitment of damaged axonal mitochondria requires PINK1

Genetic studies have indicated that PINK1 acts upstream of Parkin in the regulation of mitochondrial integrity (Clark et al., 2006; Park et al., 2006), and stabilization of PINK1 on the outer mitochondrial membrane is essential for Parkin recruitment in nonneuronal cells (Geisler et al., 2010; Narendra et al., 2010) and cell bodies of induced pluripotent stem cell–derived neurons (Seibler et al., 2011). Similarly, PINK1 is required for basal turnover of mitochondrial respiratory chain subunits in *Drosophila melanogaster* (Vincow et al., 2013). However, in the cell types examined so far, PINK1 undergoes continuous synthesis and rapid degradation in the absence of

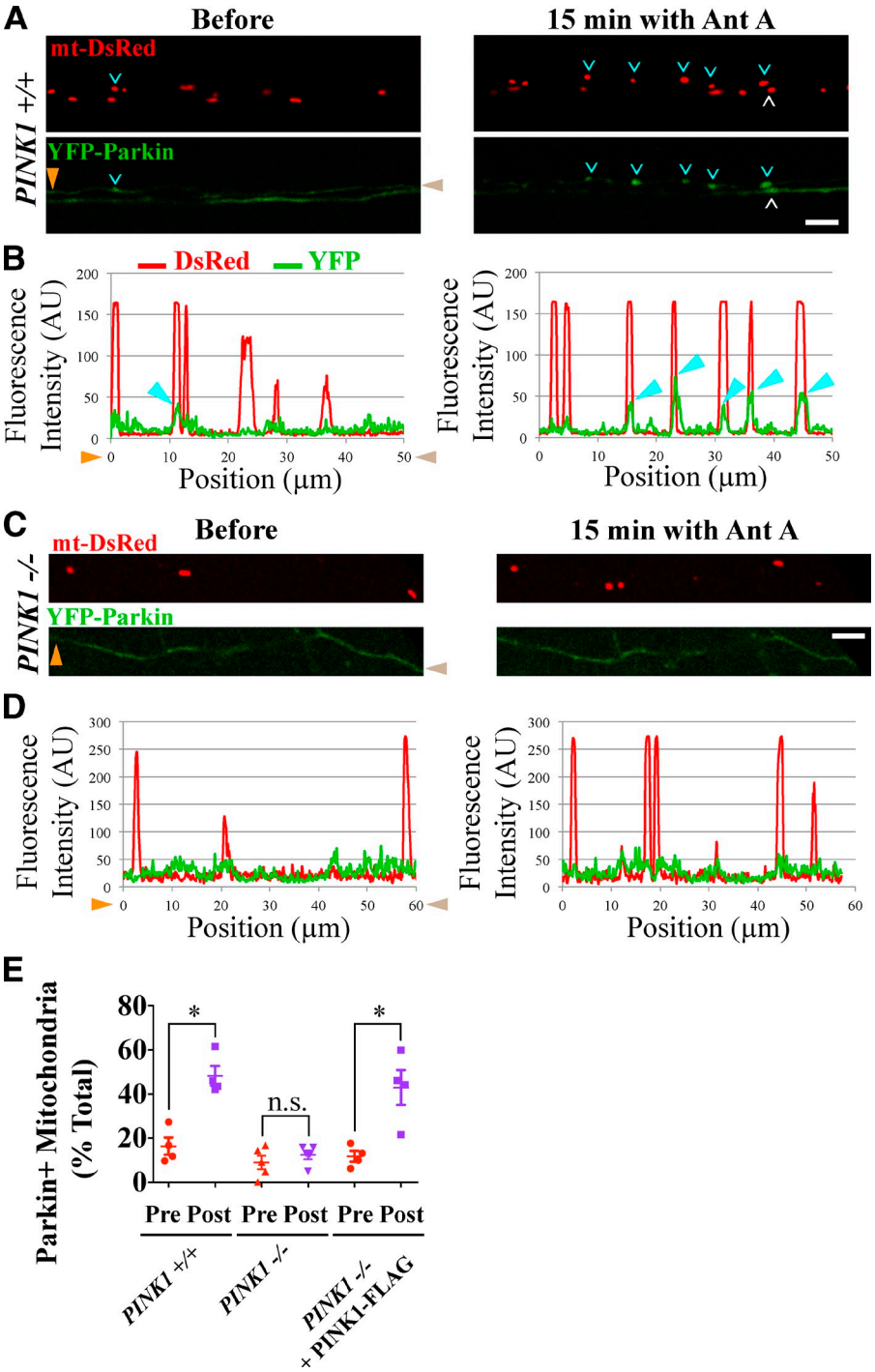

Figure 8. **Parkin recruitment to damaged axonal mitochondria requires PINK1.** (A–D) YFP-Parkin is recruited to mitochondria of *PINK1*$^{+/+}$ (A and B) but not *PINK1*$^{-/-}$ (C and D) rat hippocampal axons depolarized with 40 μM Antimycin A (Ant A). White and cyan arrowheads denote YFP-Parkin–positive mitochondria; cyan arrowheads point to mitochondria analyzed with line scans in B and D. Orange and brown arrowheads denote corresponding points in images and line scans. (E) Frequency of Parkin recruitment in the indicated genotypes before and 15 min after Antimycin A treatment. n = 87–101 mitochondria from four microfluidic devices per genotype. *, $P < 0.05$. Error bars represent means ± SEM. AU, arbitrary unit. Bars, 5 μm.

mitochondrial depolarization (Narendra et al., 2010). Because axonal transport can require days or weeks, it was uncertain whether this mechanism could pertain to distal axons. We therefore examined whether PINK1 is required for recruitment of Parkin and autophagosome membranes to axonal mitochondria. Axons of hippocampal neurons from *PINK1*$^{+/+}$ and *PINK1*$^{-/-}$ rats were treated with 40 μM Antimycin A in the perfusion chamber. In *PINK1*$^{+/+}$ axons, the percentage of YFP-Parkin–positive mitochondria increased from 16 to 48% after 20 min ($P < 0.05$; Fig. 8, A, B, and E). In contrast, YFP-Parkin failed to accumulate on Antimycin A–treated mitochondria of *PINK1*$^{-/-}$ axons (9% before and 12% after; $P = 0.5$; Fig. 8, C–E).

We had previously shown that, even in the absence of mitochondrial damage, PINK1 overexpression is sufficient to cause Parkin-dependent arrest of mitochondrial motility (Wang et al., 2011). Similarly, expression of exogenous PINK1 at high levels leads to damage-independent recruitment of Parkin to axonal mitochondria in both *PINK1*$^{+/+}$ and *PINK1*$^{-/-}$ genetic backgrounds (Fig. S4, B–E). Therefore, to rescue the recruitment of Parkin to depolarized mitochondria in *PINK1*$^{-/-}$ axons, we expressed PINK1-FLAG at low

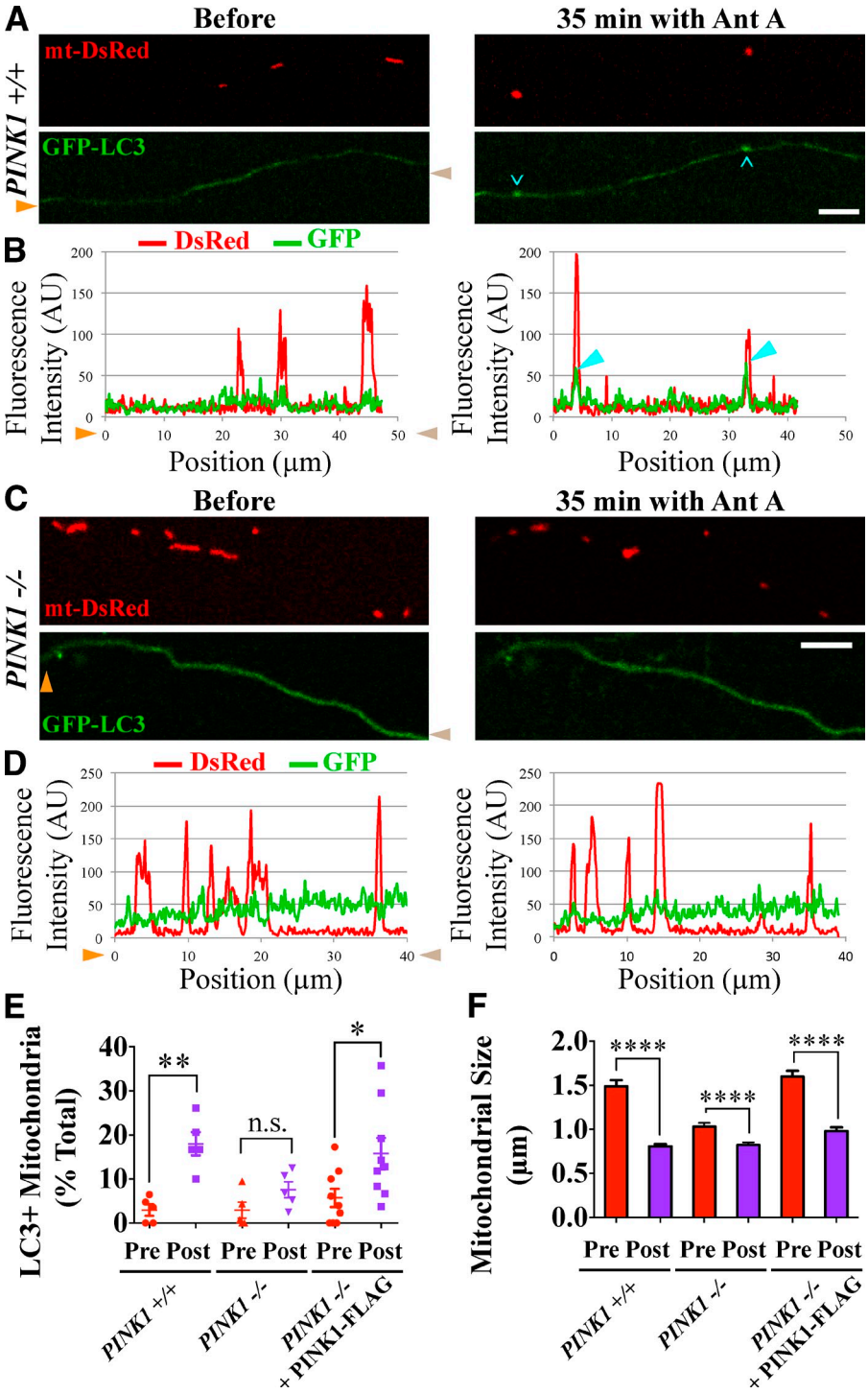

Figure 9. **Mitophagy of damaged axonal mitochondria is impaired in the absence of PINK1.** (A–D) GFP-LC3–positive autophagosomes form on mitochondria of *PINK1*$^{+/+}$ (A and B) but not *PINK1*$^{-/-}$ (C and D) rat hippocampal axons depolarized for 35 min with 40 µM Antimycin A (Ant A). (B and D) Cyan arrowheads denote GFP-LC3–positive mitochondria. (E) Frequency of autophagosome formation before and after Antimycin A treatment. Orange and brown arrowheads denote corresponding points in images and line scans. (F) Quantification of mitochondrial size before and after 20 min of Antimycin A treatment indicates that mitochondrial remodeling upon damage is PINK1 independent. Untreated mitochondria in *PINK1*$^{-/-}$ axons are smaller than those in *PINK1*$^{+/+}$ or PINK1-FLAG–expressing *PINK1*$^{-/-}$ axons. n = 108–342 mitochondria from five to nine microfluidic devices per genotype. *, $P < 0.05$; **, $P < 0.001$; ****, $P < 0.0001$. Error bars represent means ± SEM. AU, arbitrary unit. Bars, 5 µm.

enough levels to ensure cytoplasmic localization of YFP-Parkin in the absence of mitochondrial damage. In these axons, application of Antimycin A increased the fraction of Parkin-positive mitochondria from 12 to 43% ($P < 0.05$; Fig. S4, F and G; and Fig. 8 E).

We then asked whether PINK1 is similarly required for autophagosome formation on damaged mitochondria. In *PINK1*$^{+/+}$ axons, 40 µM Antimycin A increased the fraction of mitochondria colocalizing with GFP-LC3 autophagosomes from 3 to 18% ($P < 0.01$; Fig. 9, A, B, and E). In *PINK1*$^{-/-}$ axons, however, there was a smaller Antimycin A–induced change in the fractions of mitochondria colocalizing with autophagosomes (from 3 to 8%), and that change did not reach statistical significance ($P = 0.09$; Fig. 9, C–E). This represented significantly less recruitment of GFP-LC3 autophagosomes in *PINK1*$^{-/-}$ axons compared with *PINK1*$^{+/+}$ axons ($P < 0.05$). Expression of exogenous PINK1-FLAG rescued autophagosome formation on mitochondria in *PINK1*$^{-/-}$ axons. The fraction of GFP-LC3–positive mitochondria increased from 6 to 16% after Antimycin A treatment ($P < 0.05$; Fig. 9 E).

Antimycin A decreased mitochondrial size in all three genotypes ($P < 0.001$; Fig. 9 F). Despite the persistence of this morphological change, YFP-Parkin and GFP-LC3 recruitment was impaired in *PINK1*$^{-/-}$ axons, suggesting that mitochondrial accumulation of these markers is not simply caused by the altered morphology. Untreated mitochondria in *PINK1*$^{-/-}$ axons were smaller than in *PINK1*$^{+/+}$ axons as previously reported (Dagda et al., 2009), and expression of PINK1-FLAG restored the wild-type mitochondrial size in the *PINK1*$^{-/-}$ background. Our results indicate that PINK1 activates local recruitment of Parkin and initiation of mitophagy in response to mitochondrial depolarization in axons.

Discussion

Most neuronal mitochondria reside in axons and dendrites, which are also energetically demanding portions of the cell. Because mitochondrial quality control is essential for the maintenance of healthy neurons, it is important to know how damaged mitochondria are cleared from these distal compartments. In particular, although mutations in PINK1 and Parkin cause neurodegeneration, their involvement in mitochondrial clearance in axons has been controversial. The PINK1–Parkin pathway is primarily characterized in nonneuronal cells, and controversy surrounds whether it plays any role in mitochondrial quality control in neuronal processes (Van Laar et al., 2011; Wang et al., 2011; Cai et al., 2012; Grenier et al., 2013). We have now established that (a) mitophagy of damaged mitochondria occurs locally in distal neuronal axons and (b) that axonal mitophagy depends on both PINK1 and Parkin.

The study of mitochondrial quality control in neurons has been hampered by the lack of methods to induce levels of mitochondrial damage that are likely to approximate the extent of damage that might normally arise in a neuron. Other studies had previously used activation of mt-KR (Yang and Yang, 2011; Wang et al., 2012; Ertürk et al., 2014) or irradiation without a photosensitizer (Kim and Lemasters, 2011) to trigger mitophagy in nonneuronal cells. However, such methods were not applied to the sparsely distributed mitochondria in neuronal processes. Here, we used photoactivation of mt-KR to damage axonal mitochondria in a spatiotemporally controlled manner. Induction of mitochondrial damage was validated with morphological changes, such as mitochondrial fragmentation and swelling, as well as recruitment of Parkin. To damage a larger subset of axonal mitochondria, we cultured neurons in microfluidic devices that allowed local application of Antimycin A. Compared with the nonspecific ionophore CCCP, Antimycin A is a milder depolarizer and has been previously used to modulate mitochondrial motility in neurons (Miller and Sheetz, 2004; Verburg and Hollenbeck, 2008; Wang et al., 2011). Application of Antimycin A promoted rapid recruitment of YFP-Parkin to axonal mitochondria, local autophagosome formation, and lysosomal fusion, establishing axonal mitophagy as a bone fide physiological pathway. Unfortunately, antibodies are not available that can detect recruitment of endogenous Parkin in axons, and it might therefore be argued that recruitment of YFP-Parkin was a consequence of its overexpression. However, the failure of mitophagy to proceed normally in *PINK1*$^{-/-}$ rats or *Parkin*$^{-/-}$ mice indicates that the endogenous proteins are indeed necessary.

None of our protocols caused all the mitochondria to accumulate Parkin or LC3. When mt-KR was used, only a fraction of the mitochondria that were successfully depolarized acquired Parkin. Antimycin A depolarized most of the mitochondria, and yet, only 40% were scored as Parkin positive (Fig. 6 E), and 20% (Fig. 3 E) were engulfed in autophagosomes. These numbers are likely to be an underestimate because of the transient nature of mitochondrial autophagosomes, and indeed, a higher percentage of engulfed mitochondria was observed after lysosomal inhibition (Fig. 4 C). Nevertheless, in addition to depolarization, other changes in mitochondrial status may be necessary for mitophagy. The onset of mitophagy on damaged mitochondria may also be stochastic if axons can only clear a limited number of mitochondria at one time with PINK1, Parkin, or the autophagosomal machinery potentially in limiting supply. However, even restricting Antimycin A to the axonal segment within the perfusion chamber was likely to have created a greater local need for mitophagy than would arise normally in the life of the neuron.

Because the mitophagic machinery can be recruited rapidly and axonal mitochondria can lose their markers within <1 h of their depolarization, activation of the pathway should be examined acutely, and this may explain a study that failed to observe recruitment of Parkin or mitophagy in axons after extended exposure to CCCP (Cai et al., 2012). In addition, a Parkin-dependent pathway occurs in nonneuronal cells by which damaged mitochondrial proteins are selectively sequestered in mitochondrion-derived vesicles for degradation in lysosomes (Soubannier et al., 2012a,b; McLelland, et al., 2014). If this pathway functions in neurons, it may augment mitochondrial maintenance beyond the autophagic pathway analyzed here.

A prevalent model has favored transport of mitochondria toward the cell body for subsequent degradation (Miller and Sheetz, 2004). However, flux measurements in zebrafish axons indicate a bias for mitochondrial movement in the anterograde direction, suggesting that local removal of distal mitochondria must occur to maintain mitochondrial density (Plucińska et al., 2012). Similarly, when neuronal mitochondria are labeled with the fluorophore MitoTimer to determine their relative age, older mitochondria fail to return to the cell body for degradation, arguing against the retrograde transport model (Ferree et al., 2013). Our present findings that axonal mitochondria accumulate Parkin and undergo local mitophagy are consistent with the latter studies. In addition, we have previously shown that depolarization arrests mitochondrial motility by triggering PINK1–Parkin-mediated degradation of Miro, a motor–adaptor protein (Wang et al., 2011). Thus, we propose an alternative model in which acutely damaged axonal mitochondria are arrested before local mitophagy. Engulfment rather than retrograde transport of dysfunctional mitochondria would quickly isolate the organelle within the autophagosome and prevent the spread of oxidative damage during its transport.

We observed autophagosome formation along the length of the axon when mitophagy was triggered. In contrast, when

mitophagy was not triggered, autophagosome biogenesis occurred primarily in axon terminals and occasionally contained mitochondria (Maday et al., 2012). Thus, basal autophagy may serve primarily to degrade old proteins and organelles that are likely to predominate in distal axonal tips, whereas the PINK1–Parkin pathway responds to dysfunctional mitochondria anywhere along the axon.

In our study, mitoautophagosomes were largely stationary; although in agreement with previous studies (Lee et al., 2011; Maday et al., 2012), nonmitophagic autophagosomes were highly motile. Our observation of stationary mitoautophagosomes interestingly differs from the previous observation that moving autophagosomes can contain mitochondrial markers (Maday et al., 2012). One possible explanation is that stationary mitoautophagosomes may be a temporary condition: if they do not fuse with a lysosome locally, they may eventually acquire the ability to move at a later time point than we imaged after acute damage. Alternatively, autophagosomes involved in basal mitochondrial turnover in growth cones may be inherently different from those formed in response to acute activation of the PINK1–Parkin pathway.

The final step of mitophagy involves of autophagosome/lysosome fusion and enzymatic degradation of the mitochondrion (Youle and Narendra, 2011). In the present study, we found that mitoautophagosomes can undergo local maturation into autolysosomes within axons (Fig. 4). In several instances, mitochondria within autolysosomes disappeared, suggesting lysosomal acidification or degradation. The timing of their disappearance varied but could occur as early as a few minutes after colocalization with autolysosomes. Other mitochondrial autophagosomes persisted throughout the 50 min of our imaging. The robustness of this local pathway was best demonstrated by inhibiting lysosomal degradation to capture what was otherwise a transient state. With lysosomal inhibitors, fully 60% of mitochondria became LAMP1 positive 50 min after Antimycin A. We cannot exclude the possibility that some damaged mitochondria, before or after engulfment by an autophagosome, will return to the soma, particularly from proximal regions of axons and dendrites (Cai et al., 2012), and autolysosomes may eventually deliver their degraded content to the soma through retrograde transport. Local and rapid degradation of defective mitochondria, however, prevents further release of ROS throughout the cell.

Our results indicate that PINK1 is required for recruitment of Parkin to depolarized axonal mitochondria and initiation of mitophagy. But how is PINK1 activated in axons? In nonneuronal cells, loss of mitochondrial membrane potential stabilizes PINK1 by preventing its proteolysis (Narendra et al., 2010). If this mechanism is conserved in axons, constant turnover of PINK1 on healthy mitochondria and its rapid accumulation on damaged ones would require substantial amounts of PINK1 transported in a stabilized form or its abundant local synthesis de novo. It is not known whether sufficient *PINK1* mRNA is present in axons to support extensive turnover. Alternatively, the mechanism of PINK1 activation on damaged mitochondria in axons may differ from that which has been elucidated in nonneuronal mitochondria. Because PINK1 has emerged as a promising therapeutic target in PD (Hertz et al., 2013), understanding its axonal activation is particularly important.

Accumulation of mitochondrial damage in the brains of PD patients (Keeney et al., 2006; Navarro et al., 2009) and PD-like symptoms caused by mitochondrial drugs, such as Rotenone and MPTP (1-methyl-4-phenyl-1,2,3,6-tetrahydropyridine; Betarbet et al., 2000; Przedborski et al., 2004), were the first lines of evidence linking mitochondrial dysfunction to the pathology of PD. The involvement of PINK1 and Parkin in regulation of mitochondrial dynamics further supports the classification of PD as a mitochondrial disease (Chen and Chan, 2009; Wang et al., 2011). Despite the fact that dopaminergic neurons are the most pathologically affected cells in PD (Surmeier et al., 2010), the neuronal role of PINK1 and Parkin remained unclear. Moreover, because the preponderance of neuronal mitochondria resides within the axon and dendrites, it is the turnover and quality control of this population that is most likely to be relevant to the pathology. Indeed, efficient mitophagy might be more critical in axons than the soma because of the sparse and fragmented nature of axonal mitochondria and high local demand for ATP production. It is likely that axons and dendrites are the sites where PINK1 and Parkin mutations are most deleterious and the need to minimize oxidative stress from dysfunctional mitochondria is most acute.

Materials and methods

Constructs

The following constructs were used: GFP-LC3 in pBABE-puromycin vector with a SV40 promoter (gift of S.M. Thomas, Harvard Medical School, Boston, MA), YFP-Parkin and mCherry-Parkin (Narendra et al., 2008) in pEYFP-C1 and pmCherry-C1 vectors with cytomegalovirus (CMV) promoters, PINK1-FLAG in the pcDNA3.1 vector with a CMV promoter (Weihofen et al., 2009), mt-DsRed with a CMV promoter (Takara Bio Inc.), mt-GFP in the pShooter vector with a CMV promoter (gift of M. Haigis, Harvard Medical School, Boston, MA), pEGFP-N1 with a CMV promoter (Takara Bio Inc.), pKillerRed-dMito with a CMV promoter (Evrogen), and LAMP1-YFP in the pEYFP-N1 vector with a CMV promoter (plasmid 1816; Addgene; Sherer et al., 2003). mt-BFP was generated by cloning TagBFP (Evrogen) into pKillerRed-dMito to replace the KillerRed sequence.

Mice and rats

The animals used in this study were as follows: *Parkin*$^{-/-}$, strain name B6.129S4-Park2^{tm1Shn} (exon 3 deletion), and their control mice have been previously described (Goldberg et al., 2003). *PINK1*$^{-/-}$, strain name LEH-*Pink1*^{tm1sage} (26–base pair deletion in exon 4), and their control rats were of the Long–Evans hooded background (SAGE Labs). All other wild-type rats were of the Sprague–Dawley background (Charles River). Data for each genotype were obtained from embryos of three or more pregnant females.

Neuronal cell culture

Hippocampal neurons from embryonic day 18 mouse or rat embryos were dissected and dissociated as previously described (Nie and Sahin, 2012). In brief, animals were euthanized with CO_2, and embryos were removed from the abdomen. Hippocampi were dissected from embryo heads, placed in chilled dissociation medium (Ca^{2+}-free HBSS with 100 mM $MgCl_2$, 10 mM kynurenic acid, and 100 mM Hepes), and enzymatically dissociated with Papain/L-cysteine (Worthington Biochemical Corporation). Trypsin inhibitor (Sigma-Aldrich) was added, and tissue was titrated with a 5-ml pipette until clumps disappeared. Neurons were resuspended in Neurobasal medium supplemented with B27 (Gibco/Life Technologies), L-glutamine, and penicillin/streptomycin and plated at a density of $5 \times 10^4/cm^2$ on acid-etched coverslips coated overnight with 20 µg/ml poly-L-ornithine (Sigma-Aldrich) and 3.5 µg/ml laminin (Invitrogen/Life Technologies). Cultures

were maintained in the aforementioned Neurobasal medium. 4–5-d in vitro (DIV) hippocampal neurons were transfected with Lipofectamine 2000 (Invitrogen) and imaged 2–3 d later.

TCND200 or TCND500 microfluidic devices (Xona Microfluidics) were nonplasma bonded on coverslips coated overnight with 20 µg/ml poly-L-ornithine or poly-L-lysine. Dissociated hippocampal neurons were pelleted at 400 *g* for 2–3 min, resuspended at a final concentration of 4×10^4/µl in Neurobasal medium supplemented with L-glutamine and penicillin/streptomycin, plated into one of the somal compartments at a density of $5 \times 10^6/cm^2$, and cultured as previously described (Taylor et al., 2005).

For some experiments, dissociated PINK1$^{-/-}$ rat hippocampal neurons and their controls were frozen before use, stored at −140°C, and then thawed and plated in TCND200 devices at a density of $\sim 5 \times 10^6/cm^2$ according to manufacturer's protocol (KeraFAST). We did not observe any differences in the behavior of mitochondria in these previously frozen neurons from those that were plated directly after dissection.

Live imaging of neurons in microfluidic devices

Neuronal medium in microfluidic chambers was replaced with Hibernate E medium (BrainBits) and maintained at 37°C in an environmental chamber during the course of imaging. The medium in the perfusion chamber of a TCND200 device was replaced with Hibernate E containing Antimycin A (Enzo Life Sciences) at a concentration of 40 µM for rat neurons or 20 µM for mouse neurons (a lower concentration was used because mouse neurons were more sensitive to mitochondrial damage). Live imaging of YFP-, GFP-, DsRed-, and BFP-tagged markers was performed on a confocal microscope (Eclipse Ti; Nikon) equipped with an electron-multiplying charge-coupled device camera (C9100; Hamamatsu Photonics) using a 60×/NA 1.45 oil immersion lens and Volocity software (PerkinElmer). Images were captured every 1 min for a maximum of 60 min. All acquisition settings, including detector sensitivity and camera exposure time, were kept constant during imaging.

For TMRM labeling, 6–7 DIV hippocampal neurons were incubated with 20 nM TMRM (Invitrogen) in neuronal culture medium at 37°C for 20 min and imaged in Hibernate E medium containing 5 nM TMRM (Verburg and Hollenbeck, 2008). Loss of mitochondrial membrane potential was induced by adding to the perfusion chamber Hibernate E containing 40 µM Antimycin A in addition to 5 nM TMRM.

To induce excitatory stress, 9 DIV rat hippocampal neurons were treated with 250 nM Veratridine (Sigma-Aldrich) in the perfusion chamber for 10 min, and YFP-Parkin recruitment was quantified. To inhibit lysosomal degradation of damaged mitochondria, neurons were incubated with lysosomal inhibitors—5 µM Pepstatin A (Sigma-Aldrich) and 10 µm E64D (Sigma-Aldrich)—for 3–4 h before live imaging and Antimycin treatment.

Time-lapse videos of LAMP1-YFP in the axons of hippocampal neurons plated in TCND500 devices were acquired as described above. Images were collected every 2–3 s for a maximum of 2 min. 100 µm of an axon, ∼500 µm away from the cell body, was selected for analysis. Kymographs were generated from the time-lapse videos and analyzed with a custom-made ImageJ macro Kymolyzer (Supplemental material; National Institutes of Health; Pekkurnaz et al., 2014).

mt-KR activation

Before imaging, hippocampal neurons expressing mt-KR were protected from light to prevent inadvertent ROS production and apoptosis. Imaging was performed in HBSS buffer (Invitrogen) lacking antioxidants to enhance the effects of ROS produced by activated mt-KR. Hippocampal neurons could not be maintained in HBSS buffer longer than 1 h, and therefore, to visualize the formation of GFP-LC3–positive autophagosomes, Hibernate E buffer was used at the expense of lowering the efficiency of ROS production. To monitor mitochondrial membrane potential, immediately after mt-KR activation, neurons were incubated for 10 min with 20 nM TMRM in HBSS. Petri dishes containing coverslips were maintained at 37°C on a temperature-controlled stage (Heating Insert P; PeCon GmbH). Images of YFP-, GFP-, DsRed-, and BFP-tagged markers were collected on a confocal microscope (LSM 700; Carl Zeiss) equipped with photomultiplier tubes (R6357; Hamamatsu Photonics) and ZEN 2009 software (Carl Zeiss) using 63×/N.A.0.90 water IR-Achroplan objective (Carl Zeiss). To activate mt-KR, three to four mitochondria were selected in a region of interest and scanned with a 555-nm, 10-mW laser (Carl Zeiss) at 100% output 20–30× with a dwell time of 100 µs/pixel. The total length of irradiation for each region of interest did not exceed 5 min. On average, 10–12 mitochondria were bleached in three separate regions of interest in a single field of view. All acquisition settings, including detector sensitivity and camera exposure time, were kept constant during imaging.

Immunocytochemistry

Rat hippocampal neurons 5–7 DIV were fixed with 2.5% paraformaldehyde/PBS for 10 min, permeabilized with PBS containing 0.5% saponin for 1 h at room temperature, blocked with the permeabilization buffer + 1% BSA for 1 h, and incubated with mouse monoclonal anti-LAMP1 primary antibody (LY1C6; EMD Millipore) at 1:500 overnight at 4°C (Stowers et al., 2002; Glater et al., 2006). After three washes with PBS, the coverslips were incubated for 1 h at room temperature with Cy5-AffiniPure goat secondary antibody (Jackson ImmunoResearch Laboratories, Inc.) at a 1:500 dilution.

Quantification of Parkin and LC3 recruitment to mitochondria

To assess the accumulation of Parkin on mitochondria before and after 15–20 min of Antimycin A (or mock) treatment, plots of fluorescence intensity versus distance along the axon were generated for both DsRed (mitochondria) and YFP (Parkin) channels using the line scan function of ImageJ software (Schneider et al., 2012). A mitochondrion was considered Parkin positive when the relative intensity of the corresponding YFP-Parkin peak was at least twice that of the neighboring peaks. Image acquisition settings were kept constant before and after Antimycin A treatment, and analysis was performed on raw images in which brightness and contrast were adjusted identically before and after image sets. Similar analysis of Parkin accumulation was performed before and within 20 min of mt-KR or mt-DsRed activation using BFP (mitochondria) and YFP (Parkin) channels to generate line scans.

Formation of GFP-LC3 autophagosomes on mitochondria was quantified as follows: In *Parkin*$^{+/+}$ and *Parkin*$^{-/-}$ mouse hippocampal axons, the number of mitochondria colocalizing with GFP-LC3–positive puncta was counted before and 35 min after application of Antimycin A. In rat hippocampal axons, the rate of formation of GFP-LC3–positive autophagosomes was variable across different axons in different experiments. Therefore, the number of mitochondria colocalizing with GFP-LC3–positive puncta was counted before and every 5 min (≤50 min) after application of Antimycin A. The maximum percentage of LC3-positive mitochondria within 50 min was taken to represent the percentage of LC3-positive mitochondria after damage. Mock experiments, without Antimycin A treatment, were similarly analyzed.

Statistical analysis

All data are expressed as the means ± SEM. Statistical analysis and graphing were performed with Prism 6.0 for Mac OS X (GraphPad Software). The Mann–Whitney *U* test was used to determine the significance of differences between two conditions. $P < 0.05$ was considered significant and denoted with an single asterisk, whereas $P < 0.01$, $P < 0.001$, and $P < 0.0001$ are denoted with two, three, and four asterisks, respectively. In Fig. 2 D, the linear regression test was used to determine whether the slope of TMRM intensity over time was significantly different from 0.

Online supplemental material

Fig. S1 shows that irradiation of mt-DsRed does not damage mitochondria, and mitochondrial damage does not cause axonal swelling. Fig. S2 demonstrates the presence of stationary and mobile lysosomes in axons. Fig. S3 shows the recruitment of Parkin to a subset of depolarized mitochondria. Fig. S4 shows rescue of mitophagy in *Parkin*$^{-/-}$ and *PINK1*$^{-/-}$ axons by expression of Parkin and PINK1. A ZIP file is also provided that includes the source code for the Kymolyzer ImageJ macros used for generation of kymographs and determination of particle motility parameters. Online supplemental material is available at http://www.jcb.org/cgi/content/full/jcb.201401070/DC1. Additional data are available in the JCB DataViewer at http://dx.doi.org/10.1083/jcb.201401070.dv.

The authors thank S.M. Thomas, R. Youle, and M. Haigis for constructs; R. Cartoni, A. Hill, and P. Rosenberg for technical advice; and S. Vasquez and M. Sahin for assistance with hippocampal cultures.

This research was supported by National Institutes of Health GM069808 (T.L. Schwarz), the Mather's Foundation (T.L. Schwarz), Ellison Medical Foundation (T.L. Schwarz), Hartman Foundation for Parkinson's Research (T.L. Schwarz), National Institutes of Health NS065013 (M.J. LaVoie), NS069949 (M.J. LaVoie), a Howard Hughes Medical Institute International Predoctoral Fellowship (G. Ashrafi), and the Imaging and Molecular Biology Core Facilities of the Intellectual and Developmental Disabilities Center National Institutes of Health HD01866.

The authors declare no competing financial interests.

Submitted: 17 January 2014
Accepted: 26 June 2014

References

Almeida, A., J. Almeida, J.P. Bolaños, and S. Moncada. 2001. Different responses of astrocytes and neurons to nitric oxide: the role of glycolytically generated ATP in astrocyte protection. *Proc. Natl. Acad. Sci. USA*. 98:15294–15299. http://dx.doi.org/10.1073/pnas.261560998

Almeida, A., S. Moncada, and J.P. Bolaños. 2004. Nitric oxide switches on glycolysis through the AMP protein kinase and 6-phosphofructo-2-kinase pathway. *Nat. Cell Biol.* 6:45–51. http://dx.doi.org/10.1038/ncb1080

Ambrosi, G., S. Cerri, and F. Blandini. 2014. A further update on the role of excitotoxicity in the pathogenesis of Parkinson's disease. *J. Neural Transm.* http://dx.doi.org/10.1007/s00702-013-1149-z

Bains, M., and K.A. Heidenreich. 2009. Live-cell imaging of autophagy induction and autophagosome-lysosome fusion in primary cultured neurons. *Methods Enzymol.* 453:145–158. http://dx.doi.org/10.1016/S0076-6879(08)04007-X

Berger, A.K., G.P. Cortese, K.D. Amodeo, A. Weihofen, A. Letai, and M.J. LaVoie. 2009. Parkin selectively alters the intrinsic threshold for mitochondrial cytochrome c release. *Hum. Mol. Genet.* 18:4317–4328. http://dx.doi.org/10.1093/hmg/ddp384

Betarbet, R., T.B. Sherer, G. MacKenzie, M. Garcia-Osuna, A.V. Panov, and J.T. Greenamyre. 2000. Chronic systemic pesticide exposure reproduces features of Parkinson's disease. *Nat. Neurosci.* 3:1301–1306. http://dx.doi.org/10.1038/81834

Bulina, M.E., D.M. Chudakov, O.V. Britanova, Y.G. Yanushevich, D.B. Staroverov, T.V. Chepurnykh, E.M. Merzlyak, M.A. Shkrob, S. Lukyanov, and K.A. Lukyanov. 2006. A genetically encoded photosensitizer. *Nat. Biotechnol.* 24:95–99. http://dx.doi.org/10.1038/nbt1175

Burke, R.E., and K. O'Malley. 2013. Axon degeneration in Parkinson's disease. *Exp. Neurol.* 246:72–83. http://dx.doi.org/10.1016/j.expneurol.2012.01.011

Cai, Q., H.M. Zakaria, A. Simone, and Z.H. Sheng. 2012. Spatial parkin translocation and degradation of damaged mitochondria via mitophagy in live cortical neurons. *Curr. Biol.* 22:545–552. http://dx.doi.org/10.1016/j.cub.2012.02.005

Chang, D.T., A.S. Honick, and I.J. Reynolds. 2006. Mitochondrial trafficking to synapses in cultured primary cortical neurons. *J. Neurosci.* 26:7035–7045. http://dx.doi.org/10.1523/JNEUROSCI.1012-06.2006

Chen, H., and D.C. Chan. 2009. Mitochondrial dynamics—fusion, fission, movement, and mitophagy—in neurodegenerative diseases. *Hum. Mol. Genet.* 18(R2):R169–R176. http://dx.doi.org/10.1093/hmg/ddp326

Clark, I.E., M.W. Dodson, C. Jiang, J.H. Cao, J.R. Huh, J.H. Seol, S.J. Yoo, B.A. Hay, and M. Guo. 2006. *Drosophila* pink1 is required for mitochondrial function and interacts genetically with parkin. *Nature*. 441:1162–1166. http://dx.doi.org/10.1038/nature04779

Craig, A.M., and G. Banker. 1994. Neuronal polarity. *Annu. Rev. Neurosci.* 17:267–310. http://dx.doi.org/10.1146/annurev.ne.17.030194.001411

Dagda, R.K., S.J. Cherra III, S.M. Kulich, A. Tandon, D. Park, and C.T. Chu. 2009. Loss of PINK1 function promotes mitophagy through effects on oxidative stress and mitochondrial fission. *J. Biol. Chem.* 284:13843–13855. http://dx.doi.org/10.1074/jbc.M808515200

Ertürk, A., Y. Wang, and M. Sheng. 2014. Local pruning of dendrites and spines by caspase-3-dependent and proteasome-limited mechanisms. *J. Neurosci.* 34:1672–1688. http://dx.doi.org/10.1523/JNEUROSCI.3121-13.2014

Ferree, A.W., K. Trudeau, E. Zik, I.Y. Benador, G. Twig, R.A. Gottlieb, and O.S. Shirihai. 2013. MitoTimer probe reveals the impact of autophagy, fusion, and motility on subcellular distribution of young and old mitochondrial protein and on relative mitochondrial protein age. *Autophagy*. 9:1887–1896. http://dx.doi.org/10.4161/auto.26503

Geisler, S., K.M. Holmström, D. Skujat, F.C. Fiesel, O.C. Rothfuss, P.J. Kahle, and W. Springer. 2010. PINK1/Parkin-mediated mitophagy is dependent on VDAC1 and p62/SQSTM1. *Nat. Cell Biol.* 12:119–131. http://dx.doi.org/10.1038/ncb2012

Glater, E.E., L.J. Megeath, R.S. Stowers, and T.L. Schwarz. 2006. Axonal transport of mitochondria requires milton to recruit kinesin heavy chain and is light chain independent. *J. Cell Biol.* 173:545–557. http://dx.doi.org/10.1083/jcb.200601067

Goldberg, M.S., S.M. Fleming, J.J. Palacino, C. Cepeda, H.A. Lam, A. Bhatnagar, E.G. Meloni, N. Wu, L.C. Ackerson, G.J. Klapstein, et al. 2003. Parkin-deficient mice exhibit nigrostriatal deficits but not loss of dopaminergic neurons. *J. Biol. Chem.* 278:43628–43635. http://dx.doi.org/10.1074/jbc.M308947200

Greene, A.W., K. Grenier, M.A. Aguileta, S. Muise, R. Farazifard, M.E. Haque, H.M. McBride, D.S. Park, and E.A. Fon. 2012. Mitochondrial processing peptidase regulates PINK1 processing, import and Parkin recruitment. *EMBO Rep*. 13:378–385. http://dx.doi.org/10.1038/embor.2012.14

Grenier, K., G.L. McLelland, and E.A. Fon. 2013. Parkin- and PINK1-dependent mitophagy in neurons: Will the real pathway please stand up? *Front. Neurol*. 4:100. http://dx.doi.org/10.3389/fneur.2013.00100

Hertz, N.T., A. Berthet, M.L. Sos, K.S. Thorn, A.L. Burlingame, K. Nakamura, and K.M. Shokat. 2013. A neo-substrate that amplifies catalytic activity of parkinson's-disease-related kinase PINK1. *Cell*. 154:737–747. http://dx.doi.org/10.1016/j.cell.2013.07.030

Johnson, B.N., A.K. Berger, G.P. Cortese, and M.J. Lavoie. 2012a. The ubiquitin E3 ligase parkin regulates the proapoptotic function of Bax. *Proc. Natl. Acad. Sci. USA*. 109:6283–6288. http://dx.doi.org/10.1073/pnas.1113248109

Johnson, B.N., R.A. Charan, and M.J. LaVoie. 2012b. Recognizing the cooperative and independent mitochondrial functions of Parkin and PINK1. *Cell Cycle*. 11:2775–2776. http://dx.doi.org/10.4161/cc.21261

Kaasik, A., D. Safiulina, A. Zharkovsky, and V. Veksler. 2007. Regulation of mitochondrial matrix volume. *Am. J. Physiol. Cell Physiol.* 292:C157–C163. http://dx.doi.org/10.1152/ajpcell.00272.2006

Keeney, P.M., J. Xie, R.A. Capaldi, and J.P. Bennett Jr. 2006. Parkinson's disease brain mitochondrial complex I has oxidatively damaged subunits and is functionally impaired and misassembled. *J. Neurosci.* 26:5256–5264. http://dx.doi.org/10.1523/JNEUROSCI.0984-06.2006

Kim, I., and J.J. Lemasters. 2011. Mitophagy selectively degrades individual damaged mitochondria after photoirradiation. *Antioxid. Redox Signal.* 14:1919–1928. http://dx.doi.org/10.1089/ars.2010.3768

Lee, S., Y. Sato, and R.A. Nixon. 2011. Lysosomal proteolysis inhibition selectively disrupts axonal transport of degradative organelles and causes an Alzheimer's-like axonal dystrophy. *J. Neurosci.* 31:7817–7830. http://dx.doi.org/10.1523/JNEUROSCI.6412-10.2011

Legros, F., A. Lombès, P. Frachon, and M. Rojo. 2002. Mitochondrial fusion in human cells is efficient, requires the inner membrane potential, and is mediated by mitofusins. *Mol. Biol. Cell*. 13:4343–4354. http://dx.doi.org/10.1091/mbc.E02-06-0330

Maday, S., K.E. Wallace, and E.L. Holzbaur. 2012. Autophagosomes initiate distally and mature during transport toward the cell soma in primary neurons. *J. Cell Biol.* 196:407–417. http://dx.doi.org/10.1083/jcb.201106120

McLelland, G.L., V. Soubannier, C.X. Chen, H.M. McBride, and E.A. Fon. 2014. Parkin and PINK1 function in a vesicular trafficking pathway regulating mitochondrial quality control. *EMBO J.* 33:282–295.

Miller, K.E., and M.P. Sheetz. 2004. Axonal mitochondrial transport and potential are correlated. *J. Cell Sci.* 117:2791–2804. http://dx.doi.org/10.1242/jcs.01130

Mizushima, N., and M. Komatsu. 2011. Autophagy: renovation of cells and tissues. *Cell*. 147:728–741. http://dx.doi.org/10.1016/j.cell.2011.10.026

Narendra, D., A. Tanaka, D.F. Suen, and R.J. Youle. 2008. Parkin is recruited selectively to impaired mitochondria and promotes their autophagy. *J. Cell Biol.* 183:795–803. http://dx.doi.org/10.1083/jcb.200809125

Narendra, D.P., S.M. Jin, A. Tanaka, D.F. Suen, C.A. Gautier, J. Shen, M.R. Cookson, and R.J. Youle. 2010. PINK1 is selectively stabilized on impaired mitochondria to activate Parkin. *PLoS Biol.* 8:e1000298. http://dx.doi.org/10.1371/journal.pbio.1000298

Navarro, A., A. Boveris, M.J. Bández, M.J. Sánchez-Pino, C. Gómez, G. Muntané, and I. Ferrer. 2009. Human brain cortex: mitochondrial oxidative damage and adaptive response in Parkinson disease and in dementia with Lewy bodies. *Free Radic. Biol. Med.* 46:1574–1580. http://dx.doi.org/10.1016/j.freeradbiomed.2009.03.007

Nie, D., and M. Sahin. 2012. A genetic model to dissect the role of Tsc-mTORC1 in neuronal cultures. *Methods Mol. Biol.* 821:393–405. http://dx.doi.org/10.1007/978-1-61779-430-8_25

Park, J., S.B. Lee, S. Lee, Y. Kim, S. Song, S. Kim, E. Bae, J. Kim, M. Shong, J.M. Kim, and J. Chung. 2006. Mitochondrial dysfunction in *Drosophila* PINK1 mutants is complemented by parkin. *Nature*. 441:1157–1161. http://dx.doi.org/10.1038/nature04788

Parton, R.G., K. Simons, and C.G. Dotti. 1992. Axonal and dendritic endocytic pathways in cultured neurons. *J. Cell Biol.* 119:123–137. http://dx.doi.org/10.1083/jcb.119.1.123

Pekkurnaz, G., J.C. Trinidad, X. Wang, D. Kong, and T.L. Schwarz. 2014. Glucose regulates mitochondrial motility via Milton modification by *O*-GlcNAc transferase. *Cell*. 158:54–68. http://dx.doi.org/10.1016/j.cell.2014.06.007

Plucińska, G., D. Paquet, A. Hruscha, L. Godinho, C. Haass, B. Schmid, and T. Misgeld. 2012. In vivo imaging of disease-related mitochondrial dynamics in a vertebrate model system. *J. Neurosci.* 32:16203–16212. http://dx.doi.org/10.1523/JNEUROSCI.1327-12.2012

Przedborski, S., K. Tieu, C. Perier, and M. Vila. 2004. MPTP as a mitochondrial neurotoxic model of Parkinson's disease. *J. Bioenerg. Biomembr.* 36:375–379. http://dx.doi.org/10.1023/B:JOBB.0000041771.66775.d5

Rakovic, A., K. Shurkewitsch, P. Seibler, A. Grünewald, A. Zanon, J. Hagenah, D. Krainc, and C. Klein. 2013. Phosphatase and tensin homolog (PTEN)-induced putative kinase 1 (PINK1)-dependent ubiquitination of endogenous Parkin attenuates mitophagy: study in human primary fibroblasts and induced pluripotent stem cell-derived neurons. *J. Biol. Chem.* 288: 2223–2237. http://dx.doi.org/10.1074/jbc.M112.391680

Schneider, C.A., W.S. Rasband, and K.W. Eliceiri. 2012. NIH Image to ImageJ: 25 years of image analysis. *Nat. Methods*. 9:671–675. http://dx.doi.org/10.1038/nmeth.2089

Seibler, P., J. Graziotto, H. Jeong, F. Simunovic, C. Klein, and D. Krainc. 2011. Mitochondrial Parkin recruitment is impaired in neurons derived from mutant PINK1 induced pluripotent stem cells. *J. Neurosci.* 31:5970–5976. http://dx.doi.org/10.1523/JNEUROSCI.4441-10.2011

Sherer, N.M., M.J. Lehmann, L.F. Jimenez-Soto, A. Ingmundson, S.M. Horner, G. Cicchetti, P.G. Allen, M. Pypaert, J.M. Cunningham, and W. Mothes. 2003. Visualization of retroviral replication in living cells reveals budding into multivesicular bodies. *Traffic*. 4:785–801. http://dx.doi.org/10.1034/j.1600-0854.2003.00135.x

Slater, E.C. 1973. The mechanism of action of the respiratory inhibitor, antimycin. *Biochim. Biophys. Acta*. 301:129–154. http://dx.doi.org/10.1016/0304-4173(73)90002-5

Soubannier, V., G.L. McLelland, R. Zunino, E. Braschi, P. Rippstein, E.A. Fon, and H.M. McBride. 2012a. A vesicular transport pathway shuttles cargo from mitochondria to lysosomes. *Curr. Biol.* 22:135–141. http://dx.doi.org/10.1016/j.cub.2011.11.057

Soubannier, V., P. Rippstein, B.A. Kaufman, E.A. Shoubridge, and H.M. McBride. 2012b. Reconstitution of mitochondria derived vesicle formation demonstrates selective enrichment of oxidized cargo. *PLoS ONE*. 7:e52830. http://dx.doi.org/10.1371/journal.pone.0052830

Stowers, R.S., L.J. Megeath, J. Górska-Andrzejak, I.A. Meinertzhagen, and T.L. Schwarz. 2002. Axonal transport of mitochondria to synapses depends on milton, a novel *Drosophila* protein. *Neuron*. 36:1063–1077. http://dx.doi.org/10.1016/S0896-6273(02)01094-2

Surmeier, D.J., J.N. Guzman, J. Sanchez-Padilla, and J.A. Goldberg. 2010. What causes the death of dopaminergic neurons in Parkinson's disease? *Prog. Brain Res.* 183:59–77. http://dx.doi.org/10.1016/S0079-6123(10)83004-3

Taylor, A.M., M. Blurton-Jones, S.W. Rhee, D.H. Cribbs, C.W. Cotman, and N.L. Jeon. 2005. A microfluidic culture platform for CNS axonal injury, regeneration and transport. *Nat. Methods*. 2:599–605. http://dx.doi.org/10.1038/nmeth777

Taylor, A.M., D.C. Dieterich, H.T. Ito, S.A. Kim, and E.M. Schuman. 2010. Microfluidic local perfusion chambers for the visualization and manipulation of synapses. *Neuron*. 66:57–68. http://dx.doi.org/10.1016/j.neuron.2010.03.022

Van Laar, V.S., B. Arnold, S.J. Cassady, C.T. Chu, E.A. Burton, and S.B. Berman. 2011. Bioenergetics of neurons inhibit the translocation response of Parkin following rapid mitochondrial depolarization. *Hum. Mol. Genet.* 20:927–940. http://dx.doi.org/10.1093/hmg/ddq531

Verburg, J., and P.J. Hollenbeck. 2008. Mitochondrial membrane potential in axons increases with local nerve growth factor or semaphorin signaling. *J. Neurosci.* 28:8306–8315. http://dx.doi.org/10.1523/JNEUROSCI.2614-08.2008

Vincow, E.S., G. Merrihew, R.E. Thomas, N.J. Shulman, R.P. Beyer, M.J. MacCoss, and L.J. Pallanck. 2013. The PINK1-Parkin pathway promotes both mitophagy and selective respiratory chain turnover in vivo. *Proc. Natl. Acad. Sci. USA*. 110:6400–6405. http://dx.doi.org/10.1073/pnas.1221132110

Wallace, D.C. 2005. A mitochondrial paradigm of metabolic and degenerative diseases, aging, and cancer: a dawn for evolutionary medicine. *Annu. Rev. Genet.* 39:359–407. http://dx.doi.org/10.1146/annurev.genet.39.110304.095751

Wang, X., D. Winter, G. Ashrafi, J. Schlehe, Y.L. Wong, D. Selkoe, S. Rice, J. Steen, M.J. LaVoie, and T.L. Schwarz. 2011. PINK1 and Parkin target Miro for phosphorylation and degradation to arrest mitochondrial motility. *Cell*. 147:893–906. http://dx.doi.org/10.1016/j.cell.2011.10.018

Wang, Y., Y. Nartiss, B. Steipe, G.A. McQuibban, and P.K. Kim. 2012. ROS-induced mitochondrial depolarization initiates PARK2/PARKIN-dependent mitochondrial degradation by autophagy. *Autophagy*. 8:1462–1476. http://dx.doi.org/10.4161/auto.21211

Weihofen, A., K.J. Thomas, B.L. Ostaszewski, M.R. Cookson, and D.J. Selkoe. 2009. Pink1 forms a multiprotein complex with Miro and Milton, linking Pink1 function to mitochondrial trafficking. *Biochemistry*. 48:2045–2052. http://dx.doi.org/10.1021/bi8019178

Xie, Z., and D.J. Klionsky. 2007. Autophagosome formation: core machinery and adaptations. *Nat. Cell Biol.* 9:1102–1109. http://dx.doi.org/10.1038/ncb1007-1102

Yamano, K., and R.J. Youle. 2013. PINK1 is degraded through the N-end rule pathway. *Autophagy*. 9:1758–1769. http://dx.doi.org/10.4161/auto.24633

Yang, J.Y., and W.Y. Yang. 2011. Spatiotemporally controlled initiation of Parkin-mediated mitophagy within single cells. *Autophagy*. 7:1230–1238. http://dx.doi.org/10.4161/auto.7.10.16626

Youle, R.J., and D.P. Narendra. 2011. Mechanisms of mitophagy. *Nat. Rev. Mol. Cell Biol.* 12:9–14. http://dx.doi.org/10.1038/nrm3028